Soil Accumulation, Accretion, and Organic Carbon Burial Rates in Mangrove Soils of the Lower Florida Keys: A Temporal and Spatial Analysis

by

Amanda R. Chappel

A thesis submitted in partial fulfillment
Of the requirements for the degree of
Master of Science
Environmental Science & Policy
College of Arts and Sciences
University of South Florida St. Petersburg

Co-Major Professor: Joseph M. Smoak, Ph.D.
Co-Major Professor: Ryan P. Moyer, Ph.D.
Brad E. Rosenheim, Ph. D.

Date of Approval:
October 25, 2018

Keywords: mangroves, organic carbon burial, soil accumulation, radiometric dating, accretion, Florida Keys

Dedications

To my loving family, who has supported every goal and dream I have set out to achieve.

Acknowledgements

I want to thank my committee members for guiding me during this chapter of my education. I also want to thank Dr. Nicole Khan (U.S. Geological Survey, Nanyang Technical University) for providing radiocarbon data and assistance with data processing; Dr. Christian Sanders with Southern Cross University, for providing isotopic data and Dr. Mark Hester with University of Louisiana at Lafayette for graciously sharing surface elevation table data.

Further acknowledgement to Drs. Kara Radabaugh and Josh Breithaupt for always going above and beyond to help turn ideas into words. Emma Dontis, Kailey Comparetto, Ashley Huber, Jessica Jacobs, Ryan Venturelli, Dana Parkinson, Ioana Bociu, and Christina Powell for assisting with fieldwork, lab work and edits. At the Key Deer National Wildlife Refuge, Adam Emerick for granting site access and captaining us to sites and Katherine Watts for site access and permitting.

This research was possible due to funding provided by the U.S. Fish and Wildlife Service's Florida's State Wildlife Grant Program, administered through the Florida Fish and Wildlife Conservation Commission.

You all deserve ∞ beers!

TABLE OF CONTENTS

List of Tables

List of Figures

List of Equations

Abstract

This study compared the temporal variability in rates of soil accumulation, accretion, and organic carbon (OC) burial from three sites in the Lower Florida Keys using two different radiometric dating techniques (^{210}Pb, ^{14}C). Comparison of these rates across various timescales (decadal, centurial, and millennial) permitted examination of temporal responses and drivers. Further, spatial variability was measured for these associated site rates. Differences in geographic location and site morphologies as predicted, were supported by spatial variability in all rates across sites with the exception of centurial rates of accretion. All rates were greater when assessed over shorter (e.g. decadal) timescales. The centennial OC burial rates measured via ^{210}Pb during this study ranged from 106 ± 6 to 151 ± 7 g m^{-2} yr $^{-1}$. A radiocarbon-based age-depth model was constructed at Snipe Key, giving a mean OC burial rate of 39.98 ± 13.53 g m^{-2} yr^{-1}, with estimated basal peat formation beginning around 6 ka BP (mid-Holocene). The ^{14}C mean accretion rate was 0.69 ± 0.17 mm y^{-1}, whereas the ^{210}Pb mean accretion rates (10-, 50-, and 100-yr rates) ranged from 2.0 ± 0.76 to 4.2 ± 1.5 mm yr^{-1}. The 100- and 50-yr mean accretion rates were within error of the associated rates of SLR. However, rates of SLR have increased over the past ten years and are now larger than the rates of accretion required for these mangrove forests to avoid submergence. The variability associated with the larger trend of lower rates of accumulation, accretion and OC burial over longer timescales (centurial and millennial) was due to changes in sediment delivery and/or soil preservation. Stable isotopes (δ^{13}C, δ^{15}N) indicate that post-depositional transformations coupled with change in allochthonous source contribution over time were the main drivers of variability with respect to temporal rates of deposition.

Introduction

Mangrove forests are the dominant coastal wetland ecosystem in tropical and sub-tropical coastal settings, including the Florida Keys. Recent global estimates show that although mangrove forests cover less than two percent of the global surface area, they account for 10 to 15 % of the total organic carbon (OC) buried in marine environments (Twilley et al., 1992; Jennerjahn & Ittekkot, 2002; Duarte et al., 2005; Giri et al., 2011; Breithaupt et al., 2012). Coastal wetland systems have been coined "blue carbon" sinks (McLeod et al., 2011) due to their production and burial of disproportionately large quantities of OC compared to other marine environments (Donato et al., 2011; Breithaupt et al., 2012). These "blue carbon" sinks are measured and assessed in two ways, one being the OC standing stock (g m^{-2}) and the other, burial rates of OC (g m^{-2} y^{-1}). Both of these methods allow for quantification of the amount of carbon being stored in the soil at a specific depth.

Soil organic matter (SOM) is a mixture of particulate organics, humus, and charcoal among living microbial biomass and fine plant roots, a structure that has varying degrees of unfavorable substrate for enzymic mineralization (Kemmitt et al., 2008; Stockmann et al., 2013). The decomposition/preservation of these soils are controlled by biological and environmental conditions, which make the chemical composition dependent on the interplay of site conditions (moisture, temperature, etc.) and biological limitations (molecular size, specific activity, and composition; Marschner and Kalbitz, 2003; Fontaine and Bardot, 2005; Schmidt et al., 2011; Stockmann et al., 2013). The biogeochemistry of these soils is important to the preservation of SOM over different timescales, which can affect soil accumulation and OC burial rates (Table 1).

There are two major processes that support carbon storage within coastal wetlands: soil accumulation through the production and accumulation of organic matter (OM), and retaining and trapping of sediment from surrounding water flow (Furukawa et al.,1997; Saintilan et al., 2013; Krauss et al., 2014). These allochthonous and autochthonous mechanisms, which support vertical soil change, are best depicted by measuring rates rather than comparing percentages or total stocks. Measuring total stocks limits the ability to best understand the biogeochemical processes and associated effects of these soils over time as stocks strictly give a single value of carbon inventory in a system for a sampling year (Kauffman & Donato, 2012). Organic carbon burial rates often differ at various soil depths, indicating that mangrove forest soils do not sequester carbon at a continuous rate (Breithaupt et al., 2012), rather soil rates vary in space and time, as do most processes in coastal habitats. Mangrove soils are cycling reservoirs that act as tidal pump systems, where nutrients including dissolved inorganic carbon (DIC), dissolved OC (DOC) and particulate OC (POC) are transported out of the system to adjacent waters (Dittmar et al., 2006; Adame & Lovelock, 2011, Maher et al., 2013; Alongi, 2014). These processes over time can contribute to decreasing rates of accumulation and OC burial at depths.

Climate change and SLR are known to affect biogeochemical processes that influence soil accumulation and OC burial in mangrove ecosystems including carbon cycling and storage (McKee et al., 2007; Rogers & Saintilan, 2008; McKee et al., 2012; Chambers et al., 2014; Krauss et al., 2014). As climate change and SLR persist, mangrove ecosystems are expected to undergo changes in soil accumulation and carbon cycling that could compromise the system's ability to keep pace with accelerating SLR and warming temperatures (Farnsworth et al., 1996; Drexler & Ewel, 2001; Gilman et al., 2008; IPCC, 2013). In order for mangrove forests to stay within equilibrium, these systems will have to adjust to accelerating SLR by building vertically

through soil accretion, or drown through submergence (Krauss et al., 2014). Yet, the extent to which SLR will affect processes that build mangrove soils is poorly understood, and a better understanding of the potential impacts is critical to the long-term viability of mangrove ecosystems. The Lower Florida Keys are a carbonate platform system that lacks a terrestrial sediment input that many estuarine and riverine mangroves have, which is often seen as the main driver of mineral sediment and nutrient delivery (Woodroffe, 1992). These differences in geomorphic settings raise the question, how do marine sediments contribute to the process of OC burial in this system relative to other mangrove forests?

Hypotheses

When determining rates of change in soil accumulation, carbon burial, and accretion, the establishment of core chronology can vary depending upon temporal extent and dating method of interest. Lead-210 (^{210}Pb) profiles provide depositional history from decadal to centennial timescales, while carbon-14 (^{14}C) measurements on meters-thick peat deposits provide depositional history over millennial timescales. A review of previous studies indicates a strong nonlinearity of accretion and OC burial rates, which is evident when considering the different techniques and timescales (Parkinson et al., 1994; Breithaupt et al., 2018a). The first hypothesis for this study was that rates of soil accumulation, accretion, and OC burial change over time due to changes in biogeochemical processes (e.g. decomposition, degradation, and SOM production/delivery) driven by changes in sea level. Prior studies suggest that observed rates will be greater for short time periods (sub-decadal/decadal) and less for long-term time periods (centennial, millennial) (Smoak et al., 2013; Breithaupt et al., 2014; Parkinson et al., 2017; Breithaupt et al., 2018a). The use of a specific timescale when reporting rates of OC burial or projecting the future soil stability of mangrove ecosystems has profound implications

for resource managers, since understanding the appropriate timescale will allow for better adaptive management of ecosystem response to certain stressors like climate change and SLR.

Regional variability over the past century was also examined among mangrove islands sampled during this study. Physical/environmental parameters (wave energy, island slope and elevation, recurrence of and susceptibility to storm surge, anthropogenic disturbance) as well as biogeochemical processes (allochthonous material delivery, *in situ* peat production, soil density, SOM composition, decomposition/preservation rates) can influence spatial variability in these systems. The second hypothesis tested was that soil accumulation, accretion, and OC burial rates will exhibit spatial variability among mangrove islands sampled. Since other carbonate platform sites in the area have been known to receive high inputs of allochthonous sediments from storm activity, higher rates of soil accumulation, accretion, and OC burial were expected on islands more exposed to the open ocean, compared to their protected, inshore counterparts (Smoak et al., 2013; Breithaupt et al., 2014). Further, nutrient input from storms can often trigger higher density aboveground biomass, which in turn can contribute to high *in situ* peat production (Koch & Snedaker, 1997; Sanders et al., 2010; Smoak et al., 2013; Krauss et al., 2014).

Methods

Regional Setting

The Lower Florida Keys are located in the subtropical region of the western hemisphere, elongated perpendicular to the Florida shelf edge and bordered by Florida Bay (a sub-basin of the Gulf of Mexico) to the north and the Straits of Florida to the south (Fig. 1). The Lower Florida Keys have warm, humid summers and mild, dry winters with an average annual temperature of 25.4 °C and average annual rainfall of 101 cm, largely during the months of June – September (U.S. Climate Data, 2018). The local geology consists of oolite of the Miami limestone, which is comprised of bryozoan facies and oolitic facies. The oolitic facies consist of well-sorted ooids with varying amounts of skeletal material (corals, echinoids, mollusks, algae) and some quartz sand. The Miami limestone comprises the Pleistocene bedrock that exists below these mangrove islands. During the last 7,000 years, modern carbonate sand and mud have accumulated on top of the limestone supporting the recruitment of mangrove propagules (Randazzo & Jones, 1997). Due to the porous nature of the carbonate platform, submarine groundwater can be discharged vertically through the limestone and is controlled by changes in Atlantic tides relative to Florida Bay, effecting the water chemistry below these mangrove islands (Corbett et al., 2017).

The sites chosen for this study exist on protected lands that comprise part of the Florida Keys National Wildlife Refuges Complex. Hence, these mangrove forests occur in largely undeveloped areas and are protected wildlife habitats. The prevalence of intense coastal development in Southwest Florida, which often leads to changes in mangrove ecosystems, including decimation, is not a direct factor in these areas; however, there is light residential development on Big Pine and Sugarloaf Key (Figs. 2 and 4). Therefore, these near-pristine study

sites allowed quantification of the OC burial rates of relatively undisturbed systems, to best understand the mangrove ecosystems in the Lower Florida Keys.

The mangrove islands of the Florida Keys are dynamic systems that differ from mangrove habitats that exist in other areas of coastal Florida that are dominated by riverine and estuarine processes. The lower Florida Keys are subjugated by oceanic processes and lack the major source of terrigenous sediment that is found in most estuarine mangrove systems. As such, these systems have a high influx of carbonate sediments introduced by tides and storms, which can be seen as distinct overwash berms on some of the islands. The recurrence and influence of tropical cyclones can cause tree mortality, canopy gaps, wood and leaf debris, heavy sedimentation, and peat exposure, which can alter biogeochemical processes of the soils and change forest structure (Lovelock et al., 2011; Macamo et al., 2016). The most recent tropical cyclone to affect this region was hurricane Irma (Category 5, with top wind speeds of 295 km/h) in September of 2017, which caused severe tree and canopy damage as well as varying measures of storm deposition. Note that all samples for this study were collected before hurricane Irma made landfall in August 2015.

Site Selection and Study Design

The sites selected for this study occurred along a west-to-east transect extending 76 km from the Marquesas Keys to Big Pine Key in the Lower Florida Keys (Fig. 1). These sites were ideal for this study because they are relatively undisturbed mangroves systems that are accessible at high tide. Site locations, core depths, and site descriptions for each site can be found in Table 2. The westernmost site was located on the northeast side of the Marquesas Keys (LK1; Figs. 1 and 2). Working east, the next study site was located on the west side of Boca Grande Key (LK2; Figs. 1 and 2). The Mud Keys (LK3), Snipe Key (LK4 & LK7), and Waltz

Key (LK8) sites exist in relatively close proximity (<5 km), offset from Florida Bay and at the middle of the transect (Figs. 1 and 2). The two easternmost sites are located on the northern tip of Big Pine Key (LK5) and in the central section of Sugarloaf Key (LK6; Figs. 1 and 2). Both the LK5 and LK6 coring locations were established in close proximity (<10 m) to recently established surface elevation tables (SETs) (personal communication Mark Hester). These sites were dominated by red mangroves (*Rhizpohora mangle)* and black mangroves (*Avicennia germinans),* with few white mangroves (*Laguncularia racemosa).* Average canopy height at the six most southwestern sites (LK1, LK2, LK3, LK4, LK7, LK8) was 6-8 meters, however LK5 and LK6 had a canopy height of 2-3 meters dominated by scrub mangroves.

Three distinct morphologies were seen among sites, which led to the determination of spatial variability between sites that were radiometrically dated. Other site characteristics, in addition to morphology, include protection/exposure to open ocean, tidal energy, inundation periods and geographic location in relation to Peninsular Florida. Marquesas Keys represents an exposed island with dense canopy and a protected interior basin where the core was retrieved (Figs. 2 and 3). Snipe Key represents a narrow mangrove island with distinct basin and fringe settings and is less exposed than Marquesas Keys (Figs. 2 and 4). Big Pine Key was cored within the scrub mangrove fringe, which rapidly transitions into a salt barren/marsh basin (Figs. 1 and 5).

Soil Sampling and Processing

In August 2015, a 10-cm diameter polyvinyl chloride (PVC) suction-coring device was used to collect a 50-cm deep soil core at each site. Each core was taken between 10 to 250 m into the mangrove forest from the major shoreline ingress point at each site, dependent on island size and canopy density. Each core was sectioned at 2-cm intervals in the upper 10 cm, and then

at 1-cm intervals from 10 to 40-cm depth following the methods of Smoak et al. (2013). An aliquot of known volume (4.17 cm^3 for 1-cm intervals and 8.34 cm^3 for 2-cm intervals) was taken from each core interval for gravimetric analyses of dry weight and loss-on-ignition (LOI) following the methods of Ball (1964) and Craft et al. (1991). LOI is a staged combustion process that allows for soil organic matter (SOM), soil inorganic matter (SIM), and loss of carbon dioxide (LOC) to be estimated with the assumption that all SOM and carbon dioxide is combusted during their respective stages and weight from water loss is negligible after an initial drying step. Dry weight (DW) was obtained by placing samples in a drying oven at 105 ^oC for 24 hours, SOM via LOI was obtained by heating samples in a muffle furnace at 550 ^oC (W_{550}) for three hours, and LOC was obtained from a one-hour combustion at 990 ^oC (W_{990}) (Allen et al., 1974; Breithaupt et al., 2014). Weight was recorded after each treatment in grams and used to calculate each associated parameter. Dry weight was calculated from the initial crucible weight and DW following Eq. 1:

Equation 1. Dry weight equation

$$DW\ (g) = Dry\ weight\ after\ 105\ ℃\ (g) - Crucible\ weight\ (g)$$

SOM% was then calculated from the DW and W_{550} mass following Eq. 2:

Equation 2. Soil organic matter %

$$SOM\% = \ (100 * \frac{DW - W_{550}}{DW})$$

Following the SOM calculation, SIM% was calculated by subtraction SOM% from 1 following Eq. 3:

Equation 3. Soil inorganic matter %

$$SIM\% = 1 - SOM\%$$

The calculation of LOC% followed the 990 °C combustion, which is calculated from the DW, W_{550}, and W_{990} mass following Eq. 4:

Equation 4. Loss of carbon dioxide %

$$LOC\% = (100 * \frac{W_{550} - W_{990}}{DW})$$

The dry bulk density (DBD) of each soil section was then calculated by dividing the DW by the aliquot volume following Eq. 5:

Equation 5. Dry bulk density

$$DBD = \frac{DW\ (g)}{Volume\ of\ aliquot\ (cm^3)}$$

Another calculation that is important to these marine systems is the percentage of calcium carbonate ($CaCO_3$%) that is buried within the sediment deposited calculated from LOC% measured from the 990 °C combustion stage of LOI and the ratio of CO_2 in $CaCO_3$ using Eq. 6, which follows the assumption that CO_2 being liberated has negligible amounts of hydrated clays as well as other forms of carbonates (aragonite, calcite, siderite and dolomite; Davies, 1974; Dean, 1974):

Equation 6. Calcium carbonate %

$$CaCO_3\% = \frac{LOC\%}{0.44} x\ 100\ \%$$

Radiometric Analyses and Rate Calculations

Of the eight cores collected and analyzed gravimetrically, three cores, including Marquesas Keys (LK1), Big Pine Key (LK5) and Snipe Key (LK7), were radiometrically dated via gamma radiation spectroscopy (Gäggeler et al., 1976). Soil accumulation rates were determined by measuring excess ^{210}Pb ($^{210}Pb_{ex}$), a radionuclide with a half-life of 22.3 years that is well suited for studies of timescales $\leq$ 100 years (Corbett and Walsh, 2015). Measurements and calculations used to determine ^{210}Pb-derived rates of soil accumulation and OC burial were made using methods described by Smoak et al. (2013). Briefly, sectioned core intervals were freeze-dried, homogenized, and packed in gamma-counting tubes. Gamma activity was measured using an intrinsic germanium well detector coupled with a multichannel analyzer. Activity of ^{210}Pb was measured by the 46.5 kiloelectronvolts (keV) peak and radium-226 (^{226}Ra) by using its proxy ^{214}Pb by the 351.9 keV peak (Appleby et al., 1988). Counts per minute were measured and multiplied by a factor that includes the gamma-ray intensity and detector efficiency determined from standard calibrations allowing for conversion to disintegrations per minute (dpm; Smoak et al., 2013). Excess ^{210}Pb activity was calculated by subtracting the supported ^{210}Pb (i.e., ^{226}Ra activity) from the total ^{210}Pb activity. Unsupported (excess) ^{210}Pb values were determined for each sectioned layer providing an unsupported ^{210}Pb inventory for the core. The soil accumulation rates were calculated using the Constant Rate of Supply (CRS) model (Appleby & Oldfield, 1978; Smoak et al., 2013; Breithaupt et al., 2014). This model is intended for use in systems in which the initial concentration of unsupported ^{210}Pb is periodically diluted by an increase in local production or an addition of allochthonous material without excess ^{210}Pb (Appleby & Oldfield, 1978, Appleby, 2001). Thus, this model

can be applied to mangrove systems where soil deposition rates change over time while the supply rate of ^{210}Pb has remained constant over the time scale of interest. Dates derived from the bottom of each sectioned soil interval enabled the calculation of multiple rates used for this study. Mass soil accumulation rate (MAR, g m^{-2} yr^{-1}) was calculated by dividing the interval mass (g m^{-2}) by the number of years in the interval (n, yr) following Eq. 7:

Equation 7. Mass soil accumulation rate

$$MAR = \frac{interval\ mass}{n}$$

Sedimentary accretion rate (SAR, mm yr^{-1}) was calculated by dividing the interval depth (mm) by the number of years in the interval (n, yr) following Eq. 8:

Equation 8. Accretion rate

$$AR = \frac{interval\ depth}{n}$$

To account for possible autocompaction on underlying layers due to increased mass at the surface from sediment deposition, interval depths of lower bulk densities were normalized to the density of bottom layers (Lynch et al., 1989). Since no significant difference was determined between the normalized and non-normalized accretion rates for these sites, non-normalized were used herein following Eq. 8. The OC burial rate (g m^{-2} yr^{-1}), which was calculated by multiplying the MAR by the percent OC found via elemental analyzer (EA) in each interval following Eq. 9:

Equation 9. Organic carbon burial rate

$$OC\ burial\ rate = MAR\ x\ OC\%$$

The soil accumulation rates of SOM and SIM are each calculated as their respective percentages of total MAR for each interval following Eqs. 10 and 11:

Equation 10. Soil organic matter accumulation rate

$$SOM\ Accumuation\ rate = MAR\ x\ SOM\%$$

Equation 11. Soil inorganic matter accumulation rate

$$SIM\ Accumuation\ rate = MAR\ x\ SIM\%$$

Decadal Aggregation of Site-Mean Rates

The CRS model attributes dates to each sectioned soil-depth interval; however, the model dates are frequently different for corresponding depth intervals of different cores because of the varying soil accumulation rates. In order to make site-wide and SLR comparisons, the cores needed to be standardized to a common age interval (rather than depth intervals). Decadal years were used as interval boundaries and were considered as a fraction of the respective interval's age. The annual rate for each decade was then calculated as the sum of the mass within the decade, divided by ten years. A complete description of the methods and justification for use of the CRS model can be found in Smoak et al. (2013) and Breithaupt et al. (2014).

Stable Isotopes ($\delta^{13}C$ and $\delta^{15}N$), OC and TN

Soil from the core intervals described above were analyzed for total OC, total nitrogen (TN), and stable carbon and nitrogen isotope ratios ($\delta^{13}C$ and $\delta^{15}N$, respectively). Prior to analysis, samples were freeze-dried, ground to a fine power and acidified (10 % HCl) in multiple stages to remove carbonate material. Samples were then measured for the above-listed analytes using a Flash Elemental Analyzer (Thermo Flash EA 1112) coupled to a Thermo Fisher Delta V

isotope ratio mass spectrometer. Analytical precision was as follows: C = 0.1 %, N = 0.1 %, $\delta^{13}C$ = 0.1 ‰, and $\delta^{15}N$ = 0.15 ‰. Working standards for $\delta^{13}C$ were glucose, 10.7 ppt and urea, -41.3 ppt. A pair of standards were measured with every 20 samples. These standards were calibrated initially against international absolute standards LSVEC and NIST8542. Stable carbon and nitrogen isotopes are reported as ratios ($\delta^{13}C$ and $\delta^{15}N$, respectively), where delta (δ) expresses the difference of isotope ratios between samples and standard relative to the Vienna Pee Dee Belemnite (VPDB) standard for ^{13}C and atmospheric nitrogen in air for ^{15}N, in the standard permil (‰) notation relative to the standard following Eq. 12 using carbon as an example (Choi & Wang, 2004; Coplen, 2011):

Equation 12. Stable carbon and nitrogen isotopic ratio

$$\delta^{13}C = \left[\left(R_{sample}/R_{PDB}\right) - 1\right] x\ 1000$$

Following measurements of OC and SOM, a conversion factor for OC was created (Pribyl, 2010) from the three cores that were analyzed for OC using an EA. OC% and SOM% (via LOI) values from Marquesas Keys, Big Pine Key, and Snipe Key were subjected to linear regression analysis to determine a quantitative relationship between SOM estimated from LOI and direct measurements of OC for the Lower Florida Keys region (Fig. 5). The linear regression equation that describes the relationship between OC and SOM for bulk sediments (R^2 = 0.8911, p < 0.0001, n = 61) follows:

Equation 13. Site conversion factor for organic carbon

$$OC\% = (0.3702\ x\ OM) + 8.3945$$

The equation cited above is expected to provide a slightly conservative estimate of OC as a percentage of OM, however well within error. This equation was applied to remaining OM measurements within the Lower Florida Keys to give a region-specific estimate of OC values for mangrove soils.

Radiocarbon Analysis

A combination of bulk and macrofossil ^{14}C samples were measured via accelerator mass spectrometry (AMS) on a long peat core (approximately 5 m to refusal) at the Snipe Key (LK7) site. Samples were sectioned into 1-cm thick slices at 75-cm intervals between 50 and 490 cm core depth. Wet samples were then passed through a 63-μm sieve. The sample fraction > 63 μm was examined for datable macrofossils under a light-transmitted microscope and the < 63 μm fraction was collected on pre-baked (550 ^{o}C) quartz fiber filters (Whatman QFF, 0.7 μm nominal pore-size) for dating to avoid larger "young carbon" fragments and to include mangrove pollen that is used for paleoenvironmental reconstruction. Prior to graphitization, an organic base ($Na_4P_2O_4$/NaOH) was mixed with each sample to deflocculate any clays present within the sample, heated for 15 min in a water bath at 60 ^{o}C, and then centrifuged to remove the supernatant liquid. This was followed with a 10 % HCl treatment to remove carbonate materials while being heated at 85 ^{o}C and stirred, and then rinsed. The organic concentrates were then converted to graphite, pressed to targets, and analyzed via AMS at the National Ocean Sciences Accelerator Mass Spectrometry (NOSAMS) facility in Woods Hole, MA, USA (Woods Hole Oceanographic Institute, 2018). A total of 37 samples (n) were measured via AMS. Radiocarbon dates were corrected for natural isotopic fractionation and converted to calendar ages using a radiocarbon calibration program (CALIB 7.1; Stuiver et al., 2018) presenting radiocarbon dates as years before present (yr. B.P.; Stuiver & Polach, 1977;

Trumbore, 2009). The ^{14}C age-calibrated samples were within the two-standard-errors (2σ) confidence limits of expected values; but for method comparison with ^{210}Pb, one standard error (1σ) was used. In Snipe Key, 65% of the carbon was likely from marine primary production (reservoir age of 400 years) based on $\delta^{13}C$ and C:N values, and the remainder was from primary productivity from atmospheric CO_2 (no reservoir age). Thus, for sections of core above 50 cm, a mixed marine reservoir correction using these proportions was employed. This percentage of marine carbon assumed was calculated using a mixing model with a C:N endmember of 13 for marine contribution and 50 for terrestrial contribution.

Tidal Gauge Comparison

Comparing accretion rate measurements to tidal gauge records and existing projections of future SLR provides an understanding of how these systems may respond to future climate change and how carbon accumulation may be affected by future SLR. The tide gauge station used for this study was Key West, FL (station ID: 8724580), which was established in 1913, providing a 105-year tidal record (NOAA, 2017; Fig. 6). Running means were calculated from the monthly averages of mean sea level (MSL) data, which allowed for rates of SLR to be compared to accretion rates.

Surface Elevation Tables

Surface elevation tables were installed, maintained and measured by Mark Hester at the University of Louisiana Lafayette on Big Pine Key (LK5) and Sugarloaf Key (LK6) in May 2012, following USGS protocol (Cahoon & Lynch, 2010). The SETs at both sites were measured three times since installation (May 2013, September 2014, and May 2016), giving a four-yr timescale. It should be noted that no measurements were made during 2015. Net elevation change (mm) for each year of sampling is given as a mean that was calculated from

measurements taken from nine pins from each of four arms on the SET. Accretion rates were calculated following Equation 7; however, interval depth was replaced with net elevation change. This rate calculation allowed for comparison to ^{14}C and ^{210}Pb accretion rates.

Statistical Analysis

Mean and standard deviations (SD) for this study were calculated using Microsoft Excel by finding the sum of the sample ($\sum x$) then dividing by the samples' size (*n)*. Error was calculated as SD (σ). Other statistical analyses were performed using SAS® software, Version 7.1 of the SAS systems for windows (Copyright © 2016, SAS Institute Inc., Cary, NC, USA; a *p* value of < 0.05 was considered significant, normal distribution was tested prior to analysis). Soil accumulation, OC burial, and accretion rates were compared using statistical procedures that included the *t* test (paired and two-sample), Pearson's chi square, and ANOVA (Hsu & Lachenbruch, 2008). Data were tested using Brown and Forsythe's test for homogeneity of variance; if a data set had a p value < 0.05, a Welch's ANOVA was used instead of Fisher's classic one-way ANOVA. In the case of not being normally distributed, a Pearson's chi square test for independence (χ^2) was used. For *t* tests, the pooled method was used for data with equal variance and the Satterthwaite approximation was used for data with unequal variances (Radabaugh et al., 2017).

Linear regression was used to compare SOM% (via LOI) to OC% (via EA) to make an organic carbon conversion factor that could be applied to cores that were not analyzed for TOC via EA. Linear regression analysis was also applied to decadal mean accretion rates, and decadal mean rates of SLR from 1916 to 2015 (sampling year), to evaluate the relationship between variables. An exponential regression was applied to the radiocarbon dates to make an age-depth model, which includes both horizontal and vertical error bars ($\pm 1\ \sigma$).

Results

Soil Characteristics and Dating

Mean values and standard deviations for each parameter measured from gravimetric analysis (DBD, SOM%, OC%, SIM%, and $CaCO_3$%; all ± SD) are presented in Table 3. Mean DBD ranged from 0.12 ± 0.2 g cm^{-3} to 0.44 ± 0.28 g cm^{-3} among all sites. DBD for all sites was relatively uniform with the exception of Big Pine and Sugarloaf Keys (Table 3, Fig. 7). Mean SOM% ranged from 33.7 ± 20.8 to 68.9 ± 2.7 %. A negative correlation between DBD and SOM% existed for all cores as expressed by the exponential regression (Fig. 8; $p < 0.0001$). Mean SIM% range from 31.1 ± 2.7 to 66.2 ± 20.8 %. Mean OC% for all cores ranged from 20.9 ± 7.7 to 33.9 ± 1.0 %. Regression analysis was performed on SOM% and OC% values to calculate a regional conversion factor for OC (Fig. 9). Mean $CaCO_3$% ranged from 22.9 ± 5.4 to 54.6 ± 26.8 % among all sites, with the highest $CaCO_3$% values occurring in the Big Pine and Sugarloaf Keys. Each of the three cores ^{210}Pb dated showed a typical exponential decrease in specific excess ^{210}Pb down core (Fig. 10a, 10b and 10c). There was no distinct ^{137}Cs peak visible in any of these cores.

Mass Soil Accumulation Rates

Most recent decadal-averaged means of soil accumulation rates were compared between sites on the most recent 10-year (~2006-2015), 50-year (~1966-2015), and 100-year (~1916-2015) timescales (Table 4, Fig. 11). The 10-, 50-, and 100-yr mean mass accumulation rates ranged from 438 ± 18 to 906 ± 42 g m^{-2} yr^{-1}, 390 ± 18 to 682 ± 28 g m^{-2} yr^{-1}, and 302 ± 16 to 467 ± 25 g m^{-2} yr^{-1}, respectively. Statistical analysis between 10-, 50-, and 100-yr most-recent mean (including each year's aggregated rates) showed significant differences at all sites (LK1: d.f. = 2, $\chi^2 = 41.2659$, $p < 0.0001$; LK5: d.f. = 2, $\chi^2 = 38.7027$, p

< 0.0001; LK7: d.f. = 2, χ^2 = 37.0002, p < 0.0001). Accumulation rates between sites were not normally distributed nor homogeneous (natural log transformed); the Kruskal-Wallis non-parametric test was applied. Significant differences were found amongst 10-yr mean site accumulation rates (d.f. = 2, χ^2 = 26.8519, p < 0.0001) and for 100-yr mean site accumulation rates (d.f.=2, χ^2 = 51.7624, p < 0.0001). Soil accumulation rate components, SOM and SIM accumulation, were calculated to further understand the proportional make-up of accumulation rates (Table 4, Fig. 12). SOM accumulation rates ranged from 243 ± 13 to 520 ± 18 g m^{-2} yr^{-1} and SIM accumulation ranged from 92 ± 5 to 411 ± 19 g m^{-2} yr^{-1}. SOM accumulation rates were not significantly different among sites (d.f. = 2, χ^2 = 2.1595, p = 0.3397). SIM accumulation rates showed a statistical difference, supporting spatial variability (d.f. = 2, χ^2 = 25.7576, p < 0.0001).

Accretion Rates

The 10-, 50-, and 100-yr accretion rates ranged from 3.2 ± 1.04 to 4.2 ± 1.5, 2.7 ± 0.46 to 3.4 ± 1.1, and 2.0 ± 0.76 to 2.2 ± 1.1 mm yr^{-1}, respectively (Table 4, Fig 13). Statistical results show that significant differences exist, supporting temporal variability at all sites (LK1: d.f. = 2, χ^2 = 42.4642, p < 0.0001; LK5: d.f. = 2, χ^2 = 39.3306, p < 0.0001; LK7: d.f. = 2, χ^2 = 36.0101, p < 0.0001). Accretion rates between sites were not normally distributed nor homogeneous (natural log transformed); the Kruskal-Wallis non-parametric test was applied. Significant differences were found amongst 10-yr mean site accretion rates (d.f. = 2, χ^2 = 10.1446, p = 0.0063); however, no significant differences existed for the 100-yr mean site accretion rates (d.f.=2, χ^2 = 3.6554, p = 0.1608).

Mean accretion rates observed at the study sites were compared to rates of relative SLR (Fig. 13). Key West tide gauge data (est. 1913; Fig. 6) shows a trend of acceleration in more

recent years (Wdowinski, 2016). From monthly running means, rates of SLR were calculated; 10-yr mean = 8.5 ± 1.75 mm yr^{-1} (2006-2015), 50-yr mean = 2.7 ± 0.14 mm yr^{-1} (1966-2015), and 100-yr mean = 2.4 ± 0.05 mm yr^{-1} (1916-2015). To further identify changes in SLR rate variability within the most recent decade, a mean rate was calculated for 2013-2015, which was found to be 5.8 ± 7.3 mm yr^{-1}. Further, 10-year averages were calculated from sampling years 1916-2015 (Table 11). A significant difference was found between accretion and SLR rates in the most-recent 10-yr period (paired *t* test, d.f. = 2, $t = 8.43$, $p = 0.0138$), however significant differences were not found between the 50-yr most-recent means (d.f. = 2, $t = -0.86$, $p = 0.4821$) or the 100-yr most-recent means (d.f. = 2, $t = 2.79$, $p = 0.1081$). Further, regression analysis was performed to establish a mathematical relationship between accretion rates (dependent variable) and SLR rates (independent variable). The linear regression for the past 100 years from sampling year (2015; Fig. 14), yielding Eq. 14 ($R^2 = 0.35927$, $p < 0.0001$):

Equation 14. Regression equation for SLR and accretion rates

$$y = 0.1225x + 1.8518$$

Organic Carbon Burial Rates

The 10-, 50-, and 100-yr OC burial rates ranged from 158 ± 6 to 259 ± 9, 139 ± 6 to 209 ± 8, and 106 ± 6 to 151 ± 7 g m^{-2} yr^{-1}, respectively (Table 4, Fig. 15). OC burial rates at all sites were statistically tested for temporal variability between the 10-, 50-, and 100-yr most-recent means, which included each year within those means using aggregated rates. OC burial rates showed significant differences at all sites amongst timescale (LK1: d.f. = 2, $\chi^2 = 41.2659$, $p < 0.0001$; LK5: d.f. = 2, $\chi^2 = 38.7027$, $p < 0.0001$; LK7: d.f. = 2, $\chi^2 = 37.0002$, $p < 0.0001$). Organic carbon burial rates between sites were not normally distributed nor homogeneous

(natural log transformed); the Kruskal-Wallis non-parametric test was applied. Significant differences were found amongst 10-yr mean site accumulation rates (d.f. = 2, $\chi^2 = 20.4074$, $p < 0.0001$) as well as for 100-yr mean site accumulation rates (d.f.=2, $\chi^2 = 27.7238$, $p < 0.0001$).

Mean stable carbon isotope ratios ($\delta^{13}C$) measured at sites radiometrically dated were -24.6 ± 0.65 ‰ (Marquesas Keys), -21.2 ± 0.48 ‰ (Big Pine Key) and -23.22 ± 0.32 ‰ (Snipe Key) (Tables 9 & 10). Stable nitrogen isotope ratios ($\delta^{15}N$) values (measured from acidified soil samples) were -0.95 ± 1.23 ‰ (Marquesas Keys), 0.83 ± 0.66 ‰ (Big Pine Key) and 0.38 ± 0.23 ‰ (Snipe Key). Statistical difference was found amongst sites for both stable isotope ratios when tested ($\delta^{13}C$: d.f. = 2, $\chi^2 = 50.4440$, $p < 0.0001$; $\delta^{15}N$: d.f. = 2, $\chi^2 = 25.8986$, $p < 0.0001$).

Radiocarbon Age-Depth Model

The calibrated ages ranged from 616 ± 48.5 to 5659 ± 49.5 Cal yr BP giving an age-depth model with limited age discrepancies (Table 5, Fig. 16). The ^{14}C chronology from Snipe Key contained one spurious age at 124.5 cm which shows a calendar year of 4080 ± 67 Cal yr BP, an outlier on the age-depth model. Three of the deeper core intervals (485.5, 487.5 and 489.5 cm) were dated with intent to show the approximate age *in situ* mangrove peat began being deposited. However, the bulk samples at these lowest depths gave confounding ages that do not fit well with the age-depth model (Fig. 16; see Appendix 1). An exponential regression was applied to the ^{14}C age-depth model ($R^2 = 0.89511$, $p < 0.0001$), yielding Eq. 15:

Equation 15. Regression equation for ^{14}C age-depth model

$$y = 44.918e^{0.0004x}$$

This equation can be used to estimate accumulation, accretion, and OC burial rates for depth intervals that were not dated or that yielded spurious results. Calculated mean rates from the

age-depth model (Eq. 15) for accumulation, accretion and OC burial for the entire core was 89.4 ± 29.8 g m^{-2} yr^{-1}, 0.71 ± 0.14 mm yr^{-1}, and 37.4 ± 13.2 g m^{-2} yr^{-1}, respectively (Table 6).

Comparison of Rates: ^{14}C and ^{210}Pb Timescales

OC burial rates were compared on centurial and millennial timescales. For ^{210}Pb, the greatest rate of burial was detected in the 2 to 4-cm interval (7-12 years old) at 179.6 g m^{-2} yr^{-1} and lowest in the 23 to 24-cm interval (~124 years old) at 25.3 g m^{-2} y^{-1}. For ^{14}C, the greatest OC burial rate was observed in the deepest segment sampled (489-490 cm) at 80.5 g m^{-2} yr^{-1} while the lowest OC burial rate was 19.7 g m^{-2} yr^{-1} at 152-153 cm. All but three of the intervals in the top 25-cm of the core (mean ^{210}Pb burial rate = 102.2 ± 45.8 g m^{-2} yr^{-1}) had higher OC burial rates when compared to the ^{14}C carbon burial rates below 50 cm core depth (mean ^{14}C burial rate = 37.1 ± 13.5 g m^{-2} yr^{-1}). There was a significant difference found between OC burial rates of ^{210}Pb and ^{14}C (d.f. = 20.862, t = -6.27, Satterthwaite $p < 0.0001$).

Accretion rates derived from ^{210}Pb and ^{14}C dating were significantly different (d.f. = 19.503, t = -6.18, Satterthwaite $p < 0.0001$), with ^{210}Pb rates greater than the ^{14}C rates. ^{14}C accretion rates ranged from 0.51 to 1.25 mm yr^{-1}, with a mean value of 0.71 ± 0.14 mm yr^{-1} (Table 6), supporting low variability over the millennial time scale (~5043 years). ^{210}Pb accretion rates measured at Snipe Key however, show more variability over the centennial time scale, ranging from 0.49 to 4.17 mm yr^{-1}, with a mean value of 2.11 ± 1.01 mm yr^{-1} (Table 7). It should be noted that the radiocarbon dated basal intervals (485-486 cm, 487-488 cm, and 489-490 cm) from the 5-m core retrieved from Snipe Key gave spurious ages at the base of the core, which likely led to greater calculated rates of accumulation, accretion and OC burial at these depths when compared to the actual rates at these associated depths (further explanation and adjusted rates can be located in the Appendix 1).

SET Measurements

Elevation change derived from the two sites with SETs present (Big Pine and Sugarloaf Keys; Fig. 30) showed high variability over the period of time sampled (four years). Big Pine Key showed an increase in elevation of 2.28 mm with a standard error of ± 1.19 mm from 2012 to 2013, as well as an increase in elevation from 2013 to 2014 of 36.83 ± 1.90 mm, followed by a decrease in elevation change (-47.19 ± 1.68 mm) from 2014 to 2016. Sugarloaf Key had the greatest change in elevation from 2012 to 2013 of 7.41 ± 1.16 mm, followed by negligible change (-0.09 ± 0.95 mm) from 2013 to 2014, and then a 5.35 ± 0.84 mm elevation increase between 2014 to 2016. Mean accretion rates (mm yr^{-1}) calculated from the net elevation change per site, gave a rate of -0.67 ± 0.40 mm yr^{-1} for Big Pine Key (LK5) and 1.06 ± 0.25 mm yr^{-1} for Sugarloaf Key (LK6). Reference Appendix 2 for discussion on SET measurements and figure.

Discussion

Temporal Variability

Due to the extent of suitable intertidal habitat available for mangrove forests, it has been predicted that future rates of SLR could have far-reaching impacts on these systems, including submergence (Gilman et al., 2007; Gilman et al., 2008; Breithaupt et al., 2014; Phan et al., 2014; Woodroffe et al., 2016). It has been found that accretion rates in these soils vary significantly as a function of timescale, leading to bias in assessments if temporal variability is not considered (Breithaupt et al., 2018a). It was predicted that observed rates of soil accumulation, accretion, and OC burial would be higher for short-term time periods (decadal) and lower for long-term time periods (centennial, millennial; Smoak et al., 2013; Breithaupt et al., 2014; Parkinson et al., 2017; Breithaupt et al., 2018a). Coastal wetlands do not sequester carbon at a continuous rate (Breithaupt et al., 2012), and a strong nonlinearity in timescales has been previously measured (Parkinson et al., 1994; Breithaupt et al., 2014). Indeed, soil accumulation, accretion, and OC burial rates were higher for younger (shallower soil) timescales whereas lower rates were measured for older (deeper soil) timescales, following the expected trend found in the studies cited above. A high percentage of soil that accumulates in these systems goes through post-deposition transformations over time (Kirwan & Megonigal, 2013; Morris et al., 2016). During these biogeochemical transformations (i.e. diagenesis), material is degraded by the microbial communities (Holguin et al., 2001) and transported to adjacent waters largely in the form of DIC, DOC, and POC. As cycling reservoirs, mangrove soils act as tidal pumps for nutrient storage and export (Dittmar et al., 2006; Adame & Lovelock, 2011, Maher et al., 2013). Beyond biogeochemical transformations, allochthonous/autochthonous input rates are known

to change over time (Smoak et al., 2013), further impacting soil processes and characteristics at depths.

Across all sites, temporal variability was observed in all rates when compared on 10-, 50-, and 100-yr timescales (Table 4, Fig. 11-14). The lowest rates were represented by the 100-yr means and the highest rates by the 10-yr means (most recently deposited soils). As, rates of soil accumulation, accretion, and OC burial followed this same trend, the remanding discussion will use accretion rates to represent all rates for simplicity. It is suggested that temporal variability occurs over time due to many contributing factors. Newly-deposited material has a high affinity to be transformed and/or lost over time, changes in sediment delivery and/or preservation take place over time, and post-depositional transformations (biological and chemical) cycle differently over time as well (Kirwan & Megonigal, 2013; Morris et al., 2016; Breithaupt et al., 2018a). The flux observed from one interval to the next was driven by changes in soil delivery rate and/or soil degradation or removal rate (Zimmerman & Canuel, 2000; Breithaupt et al., 2014). A linear decrease was found in all rates over time for the Marquesas Keys site (Fig. 18). A decreasing step-wise function was found in all rates over time at the Snipe Key site, with signs of erosion in the more-recently deposited soil (Fig. 19). An exponential decrease was found in all rates over time at the Big Pine Key site (Fig. 20). Each of these rate/age profiles represent the amount of material present at the time of collection, where each interval represents net sedimentation (preservation/degradation). The Big Pine Key core exhibited the greatest change between the top and base of the core for all rates. This difference in rates over time could represent a change in sediment delivery or carbonate dissolution due to high rates of SIM accumulation, in particular $CaCO_3$ input, to this site (Fig. 20; Ku et al., 1999). The Snipe Key core had the lowest measured rates coupled with the least difference in rates

over time (Fig. 19). The lack of variability downcore suggests that sediment delivery was relatively constant or that soil preservation over time was higher at this site relative to the others. If the latter were to be true, consistent inundation patterns would have likely existed, allowing for anaerobic conditions to slow/retard degradation processes (McKee & Faulkner, 2000; Middleton & McKee, 2001; Saintilan et al., 2013; Krauss et al., 2014). The environmental conditions of these mangrove islands are also susceptible to erosional processes whereby carbonate dissolution and/or wave and storm energy contribute to rate change over time. Long-term erosion can lead to exposed subaerial root structures and in some cases total submergence. For example, the center lagoon of Marquesas Keys was, at one time, a mangrove forest; now these islands are erosional remnants (Fig. 3; Woodroffe et al., 2016). Distinct morphological features (exposed prop roots and lower canopy density) and lower accumulation rates in the top interval of the Snipe Key core likely represents active erosion (Fig. 19). Core retrieval at Snipe Key took place on the north side of the island, which is prone to high wind and wave energy from storms that head north through the Gulf of Mexico, supporting erosional tendencies.

This study further analyzed change in rates between centennial and millennial timescales. Carbon-14 was utilized to measure rates of accumulation, accretion, and OC burial on a millennial timescale, whereas ^{210}Pb rates were used to represent the centennial timescale. All measured rates of accumulation, accretion, and OC burial on the millennial timescale (89.3 ± 29.8 g m^{-2} yr^{-1}, 0.71 ± 0.14 mm yr^{-1}, and 37.5 ± 13.1 g m^{-2} yr^{-1}, respectively; Table 6) were lower than rates measured on the centennial timescale (293.4 ± 125.4 g m^{-2} yr^{-1}, 2.11 ± 1.01 mm yr^{-1}, and 102.7 ± 45.8 g m^{-2} yr^{-1}, respectively; Table 7, Fig. 17; strictly mean rates from Snipe Key). These results show a) rates vary over time, and/or b) longstanding degradation and post-depositional transformations continue on deeper soil intervals. The many feedback mechanisms

that take place within coastal habitats happen over different timescales and change over time (Breithaupt et al., 2018a) which can influence the timescale dependent rates measured during this study and the interpretations concluded about this system. Based on the downcore trend in accumulation, accretion, and OC burial rates, and the consistency in rates seen at depths, changes in sediment delivery and/or preservation over time, coupled with post-depositional transformation (i.e. degradation and microbial diagenesis), are likely the reasons for the difference in rates between timescales. Further, $\delta^{13}C$ values changed over both space and time, which not only suggests that delivery rates changed over time, but that sources of carbon also changed over time (Fig. 24, 25, and 26). Changes in sources can affect accumulation rates as well as OC burial rates depending on how organic-carbon rich the source may be. The 5-m peat sequence collected from Snipe Key showed increased depletion in $\delta^{13}C$ values coupled with increasing rates of OC burial downcore (Table 5 and 6, Fig. 25). This steady downcore trend in $\delta^{13}C$ and OC burial suggests a more mangrove-dominated source approaching the base of the core with $\delta^{13}C$ values and OC burial rates around -27 ‰ and 50 g m^{-2} yr^{-1}, respectively.

The agreement between geochronologies (^{14}C and ^{210}Pb) measured from Snipe Key support the trend predicted among age and rate. Although the measurements represent different timescales, agreement existed between the last dated interval from the ^{210}Pb core and the first dated interval from the ^{14}C core (Fig. 26). The ^{14}C rates measured at the 27-28 cm interval were 0.59 mm yr^{-1} (accretion) and 29.76 g m^{-2} yr^{-1} (OC burial; Table 6), while the ^{210}Pb rates measured from the 24-25 cm interval were 0.49 ± 0.36 mm yr^{-1} (accretion) and 26.92 ± 3.65 g m^{-2} yr^{-1} (OC burial; Table 7). This rate agreement further supports the timescale dependent processes that are operating over time at depth.

Spatial Variability

Differences in morphology in relation to geography and elevation existed both within and among sites. Marquesas Keys have distinct overwash berms on the exterior of the island that transition into mangrove forest basin surrounding a central lagoon (Fig. 3). In the lagoon, mangrove peat lies buried under calcareous sands and seagrass beds, evidence that mangroves that did not keep pace with SLR in the past (Macintyre et al., 2004; Woodroffe et al., 2016). Snipe Key, although narrower, has a distinct mangrove forest basin that differed in morphology from the fringe. The core was retrieved from the northern-facing fringe, the side of the island most vulnerable to sediment erosion from wave and wind energy (Fig. 5). The core on Big Pine Key was retrieved in a narrow fringe with an average tree height of 2-4 meters. Further, the elevation at Big Pine Key transitions over a short distance to support salt barren and marsh habitat approximately 15 m from the water's edge. (Fig. 4). The spatial extent of this study (76 km) was larger in comparison to other studies that sought to identify change over space in mangrove ecosystems (Callaway et al., 1997; Sanders et al., 2010; Breithaupt et al., 2014), which creates limitations when making site-wide comparisons in measured rates.

These morphological features were hypothesized to impact rates across sites, leading to the prediction that spatial variability would be observed in soil accumulation, accretion, and OC burial rates. (Lin & Sternberg, 1992; Krauss et al., 2014; Woodroffe et al., 2016). Across all sites, 100-yr mean accretion rates were not significantly different (100-yr mean of 2.31 ± 0.97 mm yr^{-1}; ± SD). It should however be noted that the degree of spatial variability increases on shorter decadal timescales, where a significant difference was found for the 10-yr mean accretion rates across all sites. These findings are similar to results found by Breithaupt et al. (2014), where spatial variability between cores decreased when rates were integrated over

longer timescales. These results are further reflected in the decreasing mean rates and associated standard deviations (Table 4). Longer timescales appear less influenced by short-term processes like erosion, remineralization, and pulse deposition events as they are integrated by long-term steady-state cycles and processes of delivery and degradation that decrease spatial variability (Breithaupt et al., 2014). This increases the likelihood of an entire site being represented by a single core, enhancing site interpretation. These morphological differences, which influence net sedimentation rate fluxes in the surface sediments, explain why significant differences were observed strictly in the decadal accretion rates.

Accretion rates, particularly in carbonate platform settings, are of interest due to the lack of mineral sediment delivery from terrigenous origins to this region which could impact accretion rates and the ability to pace sea level. Soil accumulation rates across all sites showed statistical differences, with centennial mean rates ranging from 302 ± 16 to 467 ± 25 g m^{-2} yr^{-1}. This significant difference found in accumulation rates, which did not exist for accretion rates, was further explored to see if an additive nature between organic and mineral sediment was present. There was no significant difference in 100-yr mean SOM accumulation rates across all sites (100-yr mean of 273 ± 119 g m^{-2} yr^{-1}), whereas, SIM accumulation rates were statistically different (100-yr mean of 158 ± 87 g m^{-2} yr^{-1}) over the extent of the transect. These findings are supported by those found in neighboring carbonate platform systems by Breithaupt et al. (2017), including Everglades National Park, Ten Thousand Islands, and the Yucatan Peninsula. The study found relatively small variability between SOM accumulation rates (100-yr mean of 240 ± 74 g m^{-2} yr^{-1}), yet had substantial variability in SIM accumulation rates (100-yr mean of 361 ± 470 g m^{-2} yr^{-1}) across the region, which exhibited a significant increase in mean SIM accumulation rates between soil classes (organic, intermediate, and mineral). Just as Breithaupt

et al. (2017) concluded, the contributions of SOM and SIM to soil volume and accretion at these study sites are not additive. Greater mass accumulation rates did not equate to greater accretion rates at all sites. Further, support from statistical analysis shows no significant differences in accretion rates between sites were present, while significant differences in both total soil and SIM accumulation rates. When considering accretion rates as a function of SOM accumulation (Fig. 21), a strong relationship was observed between the two rates, supporting SOM as a driver of accretion rates ($p < 0.0001$). Whereas SOM accumulation drives accretion rates, SIM accumulation was observed to drive soil density based on linear regression analysis (Fig. 22). The SIM component of dry bulk density had a high significant correlation ($p < 0.0001$) with a slope nearing 1, results consistent with Breithaupt et al. (2017).

Rates of SIM accumulation at Big Pine Key were twofold those measured at both Marquesas and Snipe Keys, where a significant difference was found across all sites (Table 4, Fig. 12 & 18-20). SOM accumulation rates however, were not significantly different among sites. Pulse events have been seen at other sites in the region (Smith et al., 2009; Smoak et al., 2013; Breithaupt et al., 2014); however, there was not a substantial decrease in excess ^{210}Pb activity nor OC%, suggesting that this is not the reason for elevated SIM input at this site. Rather, elevated SIM rates are likely due to a gradual shift in systems that are contributing to increased sediment delivery, which include but are not limited to, the movement of offshore bars and/or seagrass beds and SLR (Hine, 2013). Furthermore, the soil core taken at Big Pine Key was collected in the mangrove fringe approximately 15 m from the open water source due to scrub mangroves and salt barren occupying the island's basin (Fig. 4). Others (Chmura et al., 2003; Sanders et al., 2010) have reported higher rates of accumulation and OC burial in intertidal margins of the mangrove fringe compared to rates measured in mangrove forest

basins. Consequently, core retrieval location could also have an effect on the difference in accumulation rates among sites.

Organic Carbon Burial Rates and Stable Isotopic Ratios

The 100-yr mean OC burial rate for these three sites was 138 ± 60 g m^{-2} yr^{-1}, with site means ranging from 106 ± 6 to 151 ± 7 g m^{-2} yr^{-1}. These rates are similar to previously-reported rates for recent historical OC burial in southwest Florida. Though in a different geophysical setting, Breithaupt et al. (2018b) measured OC burial rates in the southwest coastal mangrove forests of Everglades National Park (ENP). The 100- yr regional mean OC burial rate measured was 133.8 ± 12.0 g m^{-2} yr^{-1}. This rate is very similar to the regional 100-yr mean found during this study. Breithaupt et al. (2014) also measured OC burial rates in ENP on the Shark River on six cores within a 200-m vicinity. They concluded low spatial variability on the centennial-timescale, and a mean OC burial rate of 123 ± 19 g m^{-2} yr^{-1}. This mean OC burial rate falls within the range measured during the study in the Lower Florida Keys. Furthermore, the most recent review of centennial-timescale OC burial rates that concluded a global value was Breithaupt et al. (2012); giving a mean rate of 163 g m^{-2} yr^{-1}. This value, although similar, is greater than that found in this study, with the greatest OC burial rate on the centennial-scale being 151 ± 7 g m^{-2} yr^{-1}.

Callaway et al. (1997) examined recent historical OC burial in the Upper Florida Keys adjacent to the southern tip of peninsular Florida, approximately 100 to 200 km northeast of these study sites. The study found OC burial rates of 184 ± 7.9 (red mangrove-dominated forest) and 122 ± 62 g m^{-2} yr^{-1} (black mangrove-dominated forest; applying Schumacher, 2002 OC transformation on ^{137}Cs calculated accumulation rates, approximate 33-year timescale). These rates compare best to the 50-yr mean burial rates found during this study, which range from 139

± 6 to 209 ± 8 g m^{-2} yr^{-1}. Breithaupt et al. (2017) published OC burial rates from the Yucatan Peninsula, Mexico; a carbonate platform in the southern Gulf of Mexico that has similar characteristics to these study sites in the Florida Keys, including tropical climate, distinct wet and dry seasons, and little to no terrestrial OM input. The OC burial rate measured from five sites in both basin and fringe mangroves around a sinkhole formed lagoon was 82 ± 38 g m^{-2} yr^{-1} (applying Radabaugh et al., 2017 OC transformation), rates considerably lower than rates measured during this study.

The $\delta^{13}C$ values measured during this study are likely a combination of multiple sources, thus not purely mangrove (Fig. 27). These $\delta^{13}C$ values were more enriched than those expected from strictly mangrove-derived OC peat at all sites (Fig. 24 & 25). The Marquesas Keys had a mean $\delta^{13}C$ value of -24.6 ± 0.6 ‰, followed by further enrichment at Snipe Key with a mean $\delta^{13}C$ value of -23.3 ± 0.3 ‰, and the most enriched $\delta^{13}C$ values at Big Pine Key with a mean of -21.2 ± 0.5 ‰ (Table 8). These values do not fall within the accepted range for mangrove litter of -28 to -30‰ (calculated from all available data at the time; Kristensen et al., 2008); however, are more similar to values found in mangrove forests in Brazil (basin and fringe sites) of -26 to -28‰ (Sanders et al., 2010). These results do fall within the range measured from the south Florida region of -22 to -35 ‰ (Fry and Smith, 2002); however, these sites in Everglades National Park are more influenced by terrigenous sediment. Harmon et al. (2014) measured $\delta^{13}C$ values from Dove Sound in the Upper Florida Keys that were more enriched than strictly mangrove values, which concluded source contributions from seagrass and epiphytes. This suggests that $\delta^{13}C$ values measured during this study could have come from any or all of the following to varying degrees: mangrove litter ($\delta^{13}C$ = -28 to -30 ‰), microphytobenthos ($\delta^{13}C$

= -16 to -24 ‰), seagrass ($\delta^{13}C$ = -14 to -17 ‰), and/or phytoplankton ($\delta^{13}C$ = -21 to -25 ‰; Gonneea et al., 2004; Bouillon et al., 2008; Kristensen et al., 2008).

A consistent downcore increase was measured for $\delta^{13}C$ values from the Marquesas Keys core (Fig. 24 and 25). A slight downcore increase in $\delta^{13}C$ values (1-3 ‰) is commonly seen in soil cores and it has been hypothesized to be attributed to the influence of atmospheric changes and/or preferential microbial decomposition of litter and SOM (Ehleringer et al., 2000). The enrichment downcore could also suggest that longer microbial respiration took place to depths, which induces isotope fractionation, whereby depleting mineralized CO_2 in ^{13}C while enriching degraded particulate organic matter in ^{13}C (Mariotti & Balesdent, 1990; Muzuka & Shunula, 2006; Sanders et al., 2010). The Big Pine and Snipe Keys cores show $\delta^{13}C$ variability after the 1960s, which suggests that source contributions have been changing more in recent years relative to earlier in the century, while $\delta^{13}C$ values at depths display little isotopic change since SOM degradation is less significant is areas under the water's surface (Lallier-Verges et al., 1998; Lehmann et al., 2002).

A significant difference among site $\delta^{13}C$ values was found, supporting spatial variability (Table 8, Fig. 24). Variations in $\delta^{13}C$ values along transects have been documented to be caused by post-depositional biogeochemical processes (Gonneea et al., 2004), anthropogenic influence (Gonneea et al., 2004; Harmon et al., 2014), shifts in carbon source and/or nutrient availability (Fourqurean et al. 1992; Harmon et al., 2014) and increased salt stress (Fry & Smith, 2002) in some cases. This study's transect is unique due to its extended length (76 km) and the oceanic carbonate platform setting it runs through. For these reasons, spatial variability could exist simply due to a difference in outside contributions from adjacent waters (i.e. shift in carbon source between seagrass, macroalgae, and/or phytoplankton) at each site, or morphological

differences. When exploring spatial variability in $\delta^{13}C$ values along a transect in relation to morphological differences, Lin & Sternberg (1992) found a 1 to 4 ‰ increase in $\delta^{13}C$ values along a transect that transitioned from fringe to scrub mangroves. A similar transition from to fringe to scrub mangroves was seen from Marquesas Keys to Big Pine Key. Big Pine Key had more enriched $\delta^{13}C$ values coupled with scrub-forest characteristics, including lowest average tree height and highest soil bulk density values. The differences in $\delta^{13}C$ could be a result of two edaphic conditions: 1) low groundwater levels in scrub forests make them more dependent on surface waters, which have greater seasonal differences in salinity, and 2) pore water in scrub forests often has lower concentrations of total nitrogen and phosphorous (Table 9; Lin & Sternberg, 1992). In order to determine which, if any of these suggestions are responsible for $\delta^{13}C$ enrichment along the transect, further research is needed. It is recommended that further investigation include the collection of photosynthetic gas exchange measurements, allowing for CO_2 assimilation rates to be calculated, which can be used to determine if morphological differences are the reason for $\delta^{13}C$ enrichment at Big Pine Key when compared to the other sites (Lin & Sternberg, 1992).

$\delta^{15}N$ values were more depleted than expected for mangrove soils ($\delta^{15}N$ 4 to 8 ‰, Gonneea et al., 2004). Relatively low $\delta^{15}N$ values have been measured for C3 plants like mangrove vegetation in other studies (Sanders et al., 2010). These values may also reflect nitrogen and phosphorous limitations at these sites (McKee et al., 2002). The $\delta^{15}N$ values at Marquesas Keys (-0.95 ± 1.23 ‰) were depleted relative to Snipe Key (0.38 ± 0.23 ‰) and Big Pine Key (0.83 ± 0.66 ‰; Table 9). The $\delta^{15}N$ values are comparable to values found by Harmon et al. (2014) in the upper Florida Keys of 0.43 ± 0.29‰ in the upper portion of the core (0-12 cm) and 1.17 ± 0.06‰ in the lower portion of the core (12-20 cm). A similar downcore

enrichment was found in the Big Pine Key core, representing either microbial denitrification or simply a retention of nitrogen in these soils over time (Rivera-Monroy & Twilley, 1996). A significant difference was measured between sites, with Snipe and Big Pine Keys having more enriched values when compared with Marquesas Keys. The Marquesas core was retrieved furthest into the mangrove basin, where $\delta^{15}N$ values are typically lower (Fry et al., 2000). Lower $\delta^{15}N$ values found at these sites may also be associated with high SOM concentrations as plants that selectively choose ^{14}N, thereby increasing the ^{15}N concentrations, reflect lower $\delta^{15}N$ values (Muzuka & Shunula, 2006; Sanders et al., 2010). When $\delta^{15}N$ values were graphed against $\delta^{13}C$ values, a transition to more enriched values over space was observed (Fig. 28). $\delta^{13}C/\delta^{15}N$ values increase from Marquesas Keys to Big Pine Key, which suggests that there are greater algal and allochthonous source contributions at sites closer to peninsular Florida (Sanders et al., 2014). Elevated values likely represent nitrogen cycling processes associated with more eutrophic conditions due to the addition of wastewater inputs (Costanzo et al., 2005; Harmon et al., 2014; Lapointe et al., 2004; Sanders et al., 2014).

Comparing Rates: Sea-Level Rise and Accretion

Century-mean accretion rates represented the lowest, most consistent rates for all cores, ranging between 2.0 ± 0.76 to 2.2 ± 0.90 mm yr^{-1} (Table 4, Fig. 13 & 14). These accretion rates were similar to those measured throughout the Everglades of 2.2 ± 0.1 mm yr^{-1} (century-mean accretion rates; Breithaupt et al., 2017). Accretion rates were greater on shorter timescales (10-yr mean), however, are coupled with greater variability, leading to more uncertainty and were statistically different when compared to century-mean rates and more recent SLR rates. All ^{14}C accretion rates are less than calculated rates of SLR (Table 6). This further supports the notion

of post-deposition diagenesis over long timescales, impacting rates of accretion, as sites cored during this study have kept pace with SLR historically.

A direct relationship between SLR and accretion rates in coastal wetlands is well acknowledged (McKee, 2011; Kirwan & Megonigal, 2013; Krauss et al., 2014; Woodroffe et al., 2016; Breithaupt et al., 2018a). These studies have shown that vertical change in mangrove elevation is dependent upon sea-level rise coupled with biological and physical dynamic feedbacks, both above and belowground. When compared to regional rates of SLR (Key West, FL; Station ID:8724580), the 50- and 100-yr mean accretion rates were within range (including SD) of the 50- and 100- yr rates of SLR (Fig. 13). An increase in the mean rate of SLR, from the 50-yr (2.7 ± 0.14 mm yr^{-1}) to the 10-yr (8.5 ± 1.75 mm yr^{-1}), support a trend of acceleration in more recent years (Fig. 6 & 14; Wdowinski, 2016). This rate comparison suggests these mangroves have kept pace with SLR (i.e. in equilibrium) historically; however, the more recent acceleration in sea level shows accretion rates below necessary vertical change rates (i.e. change in accretion or surface elevation) to avoid submergence (Fig. 15). Further, regression analysis was utilized to assess the influence of SLR on accretion rates. The linear regression for all sites showed that a significant relationship existed for 36 % of the data set, which follows an increasing linear trend (Fig. 14). The regression coefficient would potentially be greater if not for the dramatic increase in recent rates of SLR, while the measured accretion rates have maintained a relatively constant pattern over the past century. SLR in the past decade follows an increasing trend that ranges between 3-7 mm yr^{-1} greater that the 50-yr mean, while accretion rates have stayed relatively consistent around 2-4 mm yr^{-1} (Fig. 23). The last flux in SLR of this extent was between 1966-1975; however, accretion rates did not adjust accordingly, which

was followed by a decade with lower SLR rates. This might suggest that a lag time between SLR and accretion rates exist, and that lag time could be greater than ten years.

It is likely that the 50- and 100-yr rates of SLR underestimate the potential for these mangroves to respond through vertical change as SLR is expected to exceed equilibrium conditions (Breithaupt et al., 2018a) as predicted by historical SLR reconstructions (Gilman et al., 2007; Doyle et al., 2010; Urrego et al., 2013). Sea-level rise rates observed during the past 10 years are represented by a mean of 8.5 ± 1.75 mm yr^{-1}, rates averaging twofold that of measured accretion rates during this study (10-yr means ranged from 3.3 ± 1.1 to 4.2 ± 1.5 mm yr^{-1}). The potential for vertical soil change to keep pace with SLR is not well supported when strictly using historical reconstructions of SLR; a more recent study suggests that warming facilitates increased above- and belowground growth in mangroves that can contribute to soil elevation, in turn keeping place with SLR (Coldren et al., 2018). It should be noted that warming temperatures and SLR in this region will continue to be compounded by region-specific parameters that could further effect resiliency, thus a system's ability to pace sea level in the future. Combining measured rates from the past, with future projections, is likely the best way to predict the fate of these complex systems.

Conclusion

This study focused on quantifying soil accumulation, accretion, and OC burial rates in mangrove islands in the Lower Florida Keys. These fundamental processes are specific to these habitats, facilitating their existence in the intertidal zone. Soil cores were collected on seven mangrove islands which were exposed to a range of oceanic conditions and displayed varying morphological features. Using radiometric dating, both temporal and spatial variability were examined among measured rates. It was expected that variability would exist over both space and time. Indeed, spatial variability between rates decreased with increasing soil age, indicating that longer timescales reduce variability, while increasing the likelihood that the entirety of the site can be represented by a single soil core. Further, these findings support previous studies (Smoak et al., 2013; Breithaupt et al., 2014; Parkinson et al., 2017; Breithaupt et al., 2018a) which found that mangroves do not sequester carbon at a continuous rate, nor do different timescales compare equally. From timescale comparisons and the quantification of biogeochemical characteristics, it can be concluded that rates change over time. Change in sediment delivery and/or soil preservation over time, coupled with post-depositional transformation, are thought to be the reasons for the differences in rates among timescales. The 100-yr OC burial rates measured (regional mean of 138 ± 60 g m^{-2} yr^{-1}) compared well to other carbonate platform studies (Callaway et al., 1997; Gonneea et al., 2004; Smoak et al., 2013; Breithaupt et al., 2014; Breithaupt et al., 2018b); however, these rates are lower than the most-recent established global centennial mean for mangroves (163 g m^{-2} yr^{-1}; Breithaupt et al., 2012).

When comparing accretion rates to rates of regional SLR, it was hypothesized that more recent (2006-2015) rates of accretion would be less than recent rates of SLR (Key West, FL;

Station ID:8724580). Whereas the 50- and 100-yr mean accretion rates (2.0 ± 0.76 to 3.4 ± 1.10 mm yr^{-1}) were within range of the 50- and 100- yr mean rates of SLR (2.4 ± 0.04 to 2.7 ± 0.14 mm yr^{-1}), the 10-yr mean accretion rates (3.3 ± 1.0 to 4.2 ± 1.50 mm yr^{-1}) were well below the accelerated 10-yr mean rate of SLR (8.5 ± 1.75 mm yr^{-1}). Rate comparisons between accretion and SLR suggest mangroves in the Florida Keys have maintained equilibrium with SLR historically; however, recent accelerations in SLR show accretion rates falling below necessary vertical change rates to avoid submergence (Fig. 13; Wdowinski, 2016). Regression analysis was noticeably manipulated by the recent increase in SLR rates, supporting other studies that forecast SLR to exceed equilibrium conditions (Breithaupt et al., 2018a) as predicted by historical SLR reconstructions (Gilman et al., 2007; Doyle et al., 2010; Urrego et al., 2013).

The temporal variability observed at different timescales clearly shows the need for caution when relying on shorter timescales to make future predictions. In particular, short-term rates may only denote partial cycles rather than long-term trends (Breithaupt et al., 2014). Overestimations of system thresholds, as well as increased spatial variability, are possible when short timescales are used to represent entire site rates. For best management strategies and to accurately quantify carbon storage in a system, it is recommended that longer-term rates be taken into consideration so that more conservative predictions are made. Continued acceleration in SLR may put pressure on these mangrove islands if they are unable to keep pace with SLR through soil accretion. Considering the fate of OC is essential due the substantial quantities buried within these systems; the remobilization of once-buried OC could act as a positive feedback mechanism, perpetuating climate change, sea-level rise, and storm frequency and intensity.

Tables

Table 1. Terms Related to Accumulation and Accretion in Coastal Wetlands

Term	**Definition**
Soil accumulation	The mass of soil that accumulates in a given area per unit time (measured in g m^{-2} yr^{-1})
Soil accretion	The vertical height of material added to the soil column above a given reference plane (measured in mm yr^{-1})
Organic carbon burial	The portion of soil accumulation that strictly represents the amount of organic carbon added to the system per unit time (measured in g m^{-2} yr^{-1})
Net elevation change	The change in vertical height of the soil column above a given reference plane (impacting factors include: shrink, swell, decomposition and accretion; measured in mm yr^{-1})

Table 2. Site Locations, Core Depth, and Site Descriptions.

Site Name	Site Abbreviation	Latitude (°)	Longitude (°)	Core Depth (cm)	Site Characteristics
Marquesas Keys	LK1	24.569167	-82.102500	50	Mostly red mangroves with some black mangroves; exposed islands with dense canopy and interior protected basin
Boca Grande Key	LK2	24.532593	-82.036841	50	Mostly red mangroves with some black mangroves; exposed islands with dense canopy and interior protected basin
Snipe Key	LK3	24.676783	-81.652500	50	Mixed red/black mangrove community; protected island with dense mangrove basin among naturally channelized shoals, small in size, closer proximity to Florida Bay
Mud Keys	LK4	24.676689	-81.702014	50	Mixed red/black mangrove community with red scrubs on island interior; exposed islands with dense canopy and interior protected basin, close proximity to Florida Bay
Big Pine Key	LK5	24.693367	-81.384617	50	Dense red mangrove fringe with scrub mangrove basin (near SET); protected island with scrub mangrove shoreline and salt barren/marsh basin, close proximity to human development
Sugarloaf Key	LK6	24.678617	-81.564133	50	Dense red mangrove fringe with scrub mangrove basin (near SET); protected island with scrub mangrove shoreline and salt barren/marsh basin, close proximity to human development
Snipe Key	LK7	24.679130	-81.653140	490	Mixed red/black mangrove community; protected island with dense mangrove fringe among naturally channelized shoals, small in size, closer proximity to Florida Bay
Waltz Key	LK8	24.647500	-81.653533	50	Narrow island with mixed red/black mangrove community; protected island with dense mangrove basin among naturally channelized shoals, small in size, closer proximity to Florida Bay

Table 3. Soil Characteristics
Mean of known soil characteristics (± 1 SD) found via gravimetric analysis for each core collect from the Lower Keys for this study.

Site Location	Core Name	Core Depth (cm)	Dry Bulk Density (g cm^{-3})	Soil Organic Matter%	Organic Carbon%	Soil Inorganic Matter%	$CaCO_3$%
Marquesas Keys	LK1	40	0.20 ± 0.03	67.0 ± 3.6	33.2 ± 1.3	33.0 ± 3.6	36.2 ± 13.1
Boca Grande Key	LK2	40	0.28 ± 0.15	52.1 ± 25.8	27.6 ± 9.5	47.9 ± 25.8	42.2 ± 16.3
Snipe Key	LK3	40	0.19 ± 0.02	68.9 ± 2.7	33.9 ± 1.0	31.1 ± 2.7	22.9 ± 5.4
Mud Keys	LK4	40	0.19 ± 0.02	65.6 ± 1.9	32.7 ± 0.7	34.4 ± 2.0	38.8 ± 8.9
Big Pine Key	LK5	40	0.44 ± 0.28	33.7 ± 20.8	20.9 ± 7.7	66.2 ± 20.8	54.6 ± 26.8
Sugarloaf Key	LK6	40	0.33 ± 0.21	35.1 ± 16.4	21.4 ± 6.1	64.8 ± 16.4	44.4 ± 18.1
Snipe Key	LK7	490	0.12 ± 0.02	66.5 ± 5.4	33.1 ± 2.7	33.5 ± 5.4	34.1 ± 5.7
Waltz Key	LK8	50	0.20 ± 0.09	45.5 ± 14.1	25.2 ± 5.2	54.5 ± 14.1	50.3 ± 12.0

Table 4. Soil Accumulation, Organic Carbon Burial, and Accretion Rates
Mean rates from ^{210}Pb dating method; (± 1 SD) including mass soil accumulation (MSA), organic carbon (OC) burial, soil organic matter (SOM) accumulation, soil inorganic matter (SIM) accumulation, and accretion rates (AR). 10-yr most-recent means represents years ~2006-2015. 50-yr most-recent means represents years ~1966-2015. 100-yr most-recent means represents years ~1916-2015.

Site Name	Most Recent Mean Timescale	MSA ($g\ m^{-2}\ yr^{-1}$)	OC burial ($g\ m^{-2}\ yr^{-1}$)	SOM Accumulation ($g\ m^{-2}\ yr^{-1}$)	SIM Accumulation ($g\ m^{-2}\ yr^{-1}$)	AR ($mm\ yr^{-1}$)
Marquesas Keys	100-yr	435 ± 19	151 ± 7	309 ± 14	127 ± 5	2.0 ± 0.76
	50-yr	592 ± 24	209 ± 8	431 ± 17	161 ± 6	2.7 ± 0.46
	10-yr	699 ± 25	259 ± 9	520 ± 18	180 ± 6	3.3 ± 0.26
Big Pine Key	100-yr	467 ± 25	130 ± 7	243 ± 13	224 ± 12	2.2 ± 1.10
	50-yr	682 ± 28	201 ± 8	382 ± 16	300 ± 12	3.4 ± 1.10
	10-yr	906 ± 42	257 ± 12	494 ± 23	411 ± 19	4.2 ± 1.50
Snipe Key	100-yr	302 ± 16	106 ± 6	291 ± 16	92 ± 5	2.2 ± 0.90
	50-yr	390 ± 18	139 ± 6	298 ± 13	111 ± 5	2.8 ± 0.70
	10-yr	439 ± 18	158 ± 6	314 ± 13	124 ± 5	3.3 ± 1.0

Table 5. Radiocarbon Dates and Stable Carbon Isotope Ratios
List of radiocarbon dates in calendar years before present (Cal yr BP) from ultrafine bulk samples and macrofossils (Snipe Key-LK7) including both 1σ & 2σ (age error).

Depth interval (cm)	Type	$\delta^{13}C$	^{14}C Cal yr BP (1σ)	Error (1σ, ±)	^{14}C Cal yr BP (2σ)	Error (2σ, ±)
27-28	Bulk	-22.81	467.0	21.0	616.5	53.5
49-50	Bulk	-21.27	805.0	29.0	1074.0	96.0
65-66	Bulk	-25.72	1281.0	8.0	1278.0	18.0
83-84	Macro	-26.43	1293.5	12.5	1301.5	38.5
91-92	Macro	-25.96	1467.5	53.5	1467.0	58.0
110-111	Macro	-25.42	1567.0	34.0	1555.5	133.5
134-135	Bulk	-24.63	2022.0	31.0	2049.0	64.0
152-153	Bulk	-	2723.0	18.0	2640.5	104.5
162-163	Macro	-25.19	2633.0	94.0	2618.0	120.0
171-172	Bulk	-25.30	2723.0	18.0	2640.5	104.5
185-186	Macro	-26.27	2862.0	58.0	2858.5	66.5
197-198	Bulk	-26.99	3411.0	32.0	3408.0	39.0
197-198	Macro	-26.54	3036.5	38.5	3055.0	87.0
215-216	Macro	-25.50	3110.5	45.5	3084.5	79.5
231-232	Bulk	-26.69	3776.5	53.5	3769.0	72.0
245-246	Macro	-25.68	3933.0	35.0	3925.0	56.0
263-264	Bulk	-26.13	4067.0	75.0	4065.5	81.5
275-276	Bulk	-26.59	4194.5	40.5	4173.5	75.5
286-287	Bulk	-26.42	4356.5	58.5	4353.0	66.0
298-299	Macro	-26.28	4367.0	68.0	4401.5	108.5
313-314	Bulk	-26.52	4718.5	95.5	4715.5	106.5
313-314	Macro	-26.62	4739.5	85.5	4729.0	101.0
330-331	Bulk	-26.23	4860.5	11.5	4866.5	25.5
342-343	Macro	-27.16	4909.5	49.5	4912.5	59.5
358-359	Bulk	-26.28	4909.5	49.5	4911.5	54.5
370-371	Macro	-27.65	5364.5	65.5	5294.0	148.0
385-386	Macro	-27.31	5121.0	147.0	5089.0	196.0
399-400	Bulk	-26.64	5449.5	119.5	5451.5	125.5
422-423	Bulk	-26.51	5190.5	116.5	5183.5	129.5
422-423	Macro	-27.24	5617.0	24.0	5617.5	27.5
437-438	Bulk	-27.27	5186.5	113.5	5181.0	126.0
454-455	Macro	-27.10	5544.0	55.0	5544.0	63.0
464-465	Macro	-28.12	5659.5	49.5	5662.5	57.5
485-486	Bulk	-26.34	4738.5	87.5	4728.0	104.0
487-488	Bulk	-25.78	4506.5	60.5	4508.0	69.0
489-490	Bulk	-24.08	3916.0	44.0	3908.0	63.0

Table 6. Radiocarbon Soil Characteristics and Rates
Measured and calculated accretion rates (AR), total organic carbon (TOC) percentage, dry bulk density (DBD), organic carbon (OC) burial rates, and mass accumulation rates (MAR) for Snipe Key radiocarbon (^{14}C) dates.

Depth (cm)	AR (mm yr^{-1})	TOC (%)	DBD (g cm^{-3})	OC burial rates (g m^{-2} y^{-1})	MAR (g m^{-2} y^{-1})
27-28	0.589	34.86	0.145	29.765	85.385
49-50	0.615	28.10	0.156	26.955	95.925
65-66	0.511	40.26	0.119	24.497	60.847
83-84	0.646	42.86	0.102	28.221	65.845
91-92	0.624	30.29	0.121	22.854	75.445
110-111	0.705	27.70	0.131	25.591	92.377
134-135	0.665	30.81	0.155	31.766	103.103
152-153	0.560	31.25	0.113	19.777	63.285
162-163	0.617	48.28	0.151	44.993	93.192
171-172	0.630	32.35	0.120	24.452	75.578
185-186	0.648	31.72	0.118	24.257	76.481
197-198	0.579	45.98	0.092	24.493	53.269
197-198	0.650	45.98	0.092	27.514	59.839
215-216	0.693	40.90	0.163	46.188	112.929
231-232	0.613	33.46	0.115	23.589	70.495
245-246	0.624	49.70	0.135	41.881	84.268
263-264	0.648	52.15	0.148	50.006	95.889
275-276	0.657	35.77	0.115	27.018	75.533
286-287	0.658	35.82	0.125	29.442	82.205
298-299	0.684	52.68	0.107	38.529	73.138
313-314	0.664	53.16	0.103	36.379	68.434
313-314	0.661	53.16	0.103	36.218	68.131
330-331	0.680	37.59	0.128	32.713	87.036
342-343	0.698	52.79	0.120	44.193	83.715
358-359	0.730	52.15	0.111	42.270	81.054
370-371	0.691	52.15	0.149	53.666	102.907
385-386	0.753	53.04	0.135	53.902	101.626
399-400	0.733	54.15	0.092	36.521	67.445
422-423	0.814	36.99	0.109	32.821	88.725
422-423	0.752	36.99	0.109	30.329	81.988
437-438	0.844	56.36	0.111	52.771	93.633
454-455	0.820	53.56	0.119	52.251	97.557
464-465	0.821	46.27	0.109	41.394	89.461
485-486	1.025	37.45	0.136	52.184	139.344
487-488	1.082	37.45	0.144	58.338	155.775
489-490	1.250	37.45	0.172	80.518	215.000
Mean	*0.712*	*41.81*	*0.125*	*37.452*	*89.357*

Table 7. Rates of Soil Accumulation, Organic Carbon Burial, and Accretion of Snipe Key
Downcore rate calculations via ^{210}Pb dating for Snipe Key (LK7) including mass soil accumulation (MSA), accretion rates (AR) and organic carbon (OC) burial. Error calculated from CRS model (1σ).

Depth (cm)	MSA rates ($g\ m^{-2}\ yr^{-1}$)	MSA error ($g\ m^{-2}\ yr^{-1}$)	AR ($mm\ yr^{-1}$)	AR error ($mm\ yr^{-1}$)	OC burial rates ($g\ m^{-2}\ yr^{-1}$)	OC burial error ($g\ m^{-2}\ yr^{-1}$)
0-2	403.98	20.14	2.70	0.03	144.12	7.18
2-4	491.73	15.68	4.17	0.03	179.57	5.73
4-6	419.35	18.59	3.85	0.03	147.15	6.52
6-8	350.28	13.74	3.38	0.03	125.12	4.91
8-10	392.17	18.21	2.77	0.03	137.37	6.38
10-11	376.64	16.94	2.58	0.07	134.69	6.06
11-12	409.82	19.77	2.71	0.07	143.25	6.91
12-13	364.33	17.45	2.30	0.08	132.06	6.32
13-14	353.88	15.19	2.05	0.08	125.81	5.40
14-15	342.18	20.20	1.86	0.08	119.61	7.06
15-16	427.70	27.85	2.80	0.09	147.61	9.61
16-17	282.18	16.74	1.94	0.09	96.96	5.75
17-18	186.03	9.14	1.55	0.10	61.04	3.00
18-19	190.98	10.93	1.48	0.11	63.66	3.64
19-20	178.37	11.38	1.18	0.13	60.68	3.87
20-21	165.41	12.06	1.19	0.15	56.03	4.08
21-22	164.47	14.87	1.03	0.18	55.77	5.04
22-23	215.97	31.42	1.69	0.18	72.03	10.48
23-24	74.78	6.77	0.58	0.26	25.25	2.29
24-25	77.23	10.46	0.49	0.36	26.92	3.65
Mean	*293.37*	-	*2.11*	-	*102.73*	-

Table 8. Stable Carbon Isotopic Ratios and Total Organic Carbon
$\delta^{13}C$ values and total organic carbon (TOC) percentage for Marquesas Keys (LK1), Big Pine Key (LK5) and Snipe Key (LK7), including the top 25 cm of each core.

Depth	**LK1 - Marquesas Keys**		**LK5 – Big Pine Key**		**LK7 - Snipe Key**	
(cm)	**$\delta^{13}C$**	**TOC%**	**$\delta^{13}C$**	**TOC%**	**$\delta^{13}C$**	**TOC%**
0-2	-25.6	38.09	-21.4	30.22	-23.5	35.68
2-4	-25.7	35.95	-20.5	27.00	-23.7	36.52
4-6	-25.8	36.29	-20.7	29.58	-23.9	35.09
6-8	-25.1	33.31	-20.3	30.15	-23.6	35.72
8-10	-25.6	34.70	-20.6	29.05	-23.3	35.03
10-11	-24.6	33.67	-21.5	30.91	-23.0	35.76
11-12	-24.7	34.40	-21.8	30.67	-23.3	34.96
12-13	-24.6	34.72	-21.6	29.37	-23.0	36.25
13-14	-24.1	34.16	-21.6	28.98	-23.8	35.55
14-15	-24.3	34.21	-21.3	27.54	-23.3	34.95
15-16	-24.4	33.22	-20.7	26.44	-23.2	34.51
16-17	-24.0	33.64	-20.7	23.67	-22.6	34.36
17-18	-24.3	32.74	-21.3	25.07	-23.0	32.81
18-19	-23.7	32.38	-21.5	26.03	-23.0	33.34
19-20	-24.2	32.24	-21.5	26.05	-23.3	34.02
20-21	-24.0	33.01	-21.5	23.07	-23.1	33.88
21-22	-24.3	32.84	-21.4	24.87	-23.3	33.91
22-23	-24.3	31.65	-21.6	25.87	-23.1	33.35
23-24	-24.0	31.77	-21.8	22.78	-23.5	33.76
24-25	-	-	-	-	-23.5	34.86
Mean	***-24.6***	***33.80***	***-21.2***	***27.3***	***-23.22***	***34.16***

Table 9. Stable Nitrogen Isotope Ratios and Total Nitrogen
Measured $\delta^{15}N$ values and total nitrogen (TN) percentages for Marquesas Keys (LK1), Big Pine Key (LK5) and Snipe Key (LK7), including the top 25 cm of each core.

Depth	**LK1 - Marquesas Keys**		**LK5 – Big Pine Key**		**LK7 - Snipe Key**	
(cm)	**$\delta^{15}N$**	**%TN**	**$\delta^{15}N$**	**%TN**	**$\delta^{15}N$**	**%TN**
0-2	-1.2	1.86	-0.5	1.86	0.3	1.75
2-4	-0.4	1.83	-0.3	1.68	0.5	1.76
4-6	-1.7	1.82	-0.3	1.95	0.2	1.67
6-8	-3.5	1.79	0.3	1.99	0.3	1.76
8-10	0.6	1.43	0.6	1.89	0.5	1.73
10-11	-2.0	1.76	1.3	1.87	0.3	1.83
11-12	-1.9	1.72	1.2	1.82	0.0	1.72
12-13	-2.0	1.73	1.6	1.79	0.3	1.56
13-14	0.8	1.51	1.4	1.69	0.8	1.61
14-15	-2.4	1.61	1.3	1.35	0.7	1.49
15-16	-2.6	1.59	1.3	1.40	0.6	1.52
16-17	-0.8	1.60	1.5	1.22	0.3	1.47
17-18	-0.5	1.45	0.7	1.17	0.5	1.43
18-19	-0.5	1.46	0.6	1.09	0.7	1.45
19-20	-0.1	1.42	0.3	1.13	0.0	1.38
20-21	0.2	1.42	1.2	0.92	0.4	1.45
21-22	0.0	1.32	1.3	1.03	0.1	1.48
22-23	0.5	1.29	1.2	1.01	0.2	1.39
23-24	-0.3	1.44	1.0	0.78	0.6	1.31
24-25	-	-	-	-	0.4	1.36
Mean	***-0.95***	***1.58***	***0.83***	***1.45***	***0.38***	***1.55***

Table 10. Calculated Ten-Year Mean Rates of Sea-Level Rise
Mean rates of sea-level rise (SLR) calculated from monthly running mean sea level data collected from the Key West tide gauge (Station ID: 8724580).

Year Interval	Mean rate of SLR
2015-2006	8.52
2005-1996	3.67
1995-1986	4.82
1985-1976	5.37
1975-1966	8.19
1965-1956	-3.20
1955-1946	-4.93
1945-1936	0.56
1935-1926	4.39
1925-1916	-3.01

Table 11. Spurious Radiocarbon Age and Rates
Due to confounding ages, certain intervals were reexamined for estimated age and rates (Reference equation 18).

Depth (cm)	Type	Adjusted age from equation (Cal yr BP)	Estimated OC burial rates from equation (g $m^{-2}yr^{-1}$)	Estimated accretion rates from equation (mm yr^{-1})
124.5	Outlier	2605	17.27	0.48
485.5	Base segment	6007	41.16	0.80
487.5	Base segment	6017	43.69	0.81
489.5	Base segment	6028	52.30	0.81

Figures

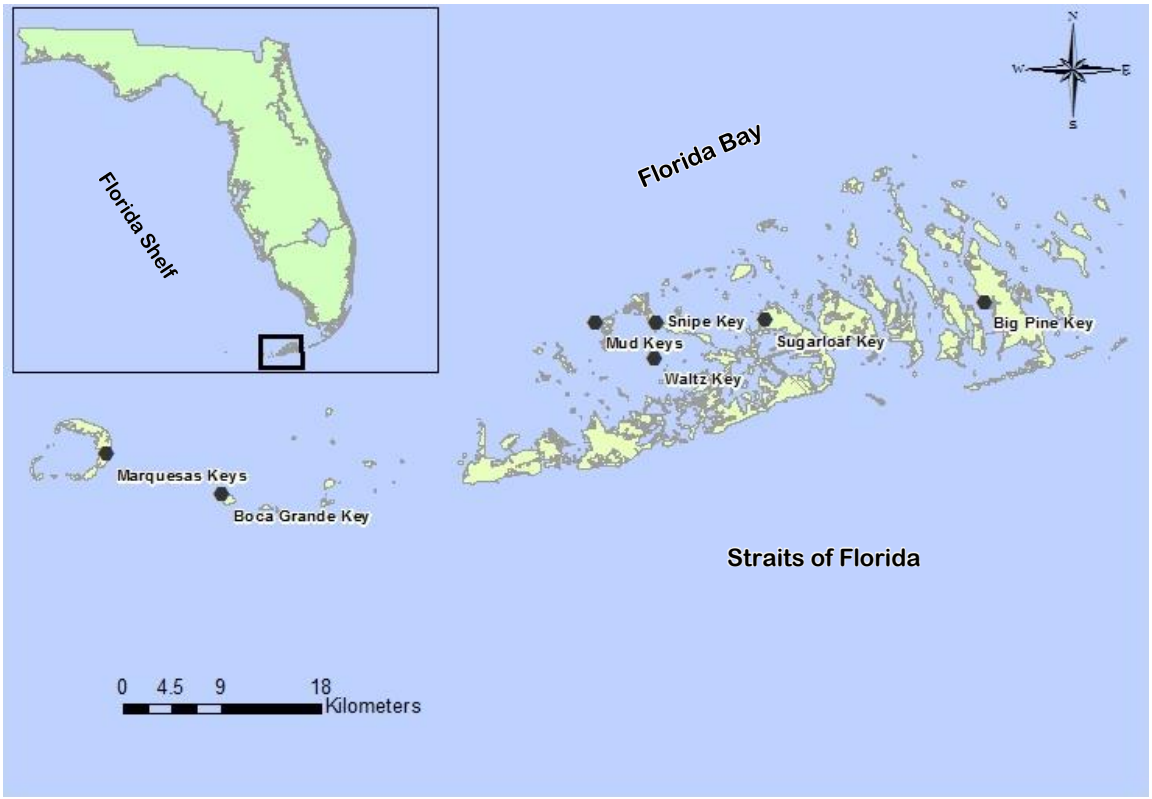

Figure 1. Site Map
Locations of mangrove islands in the Lower Florida Keys that were sampled for soil cores.

Figure 2. Satellite Site Map
Coring sites represented with yellow circles. Source: Esri, DigitalGlobe, GeoEye, Earthstar Geographics, CNES/Airbus DS, USDA, USGS, AeroGRID, IGN, and the GIS user community.

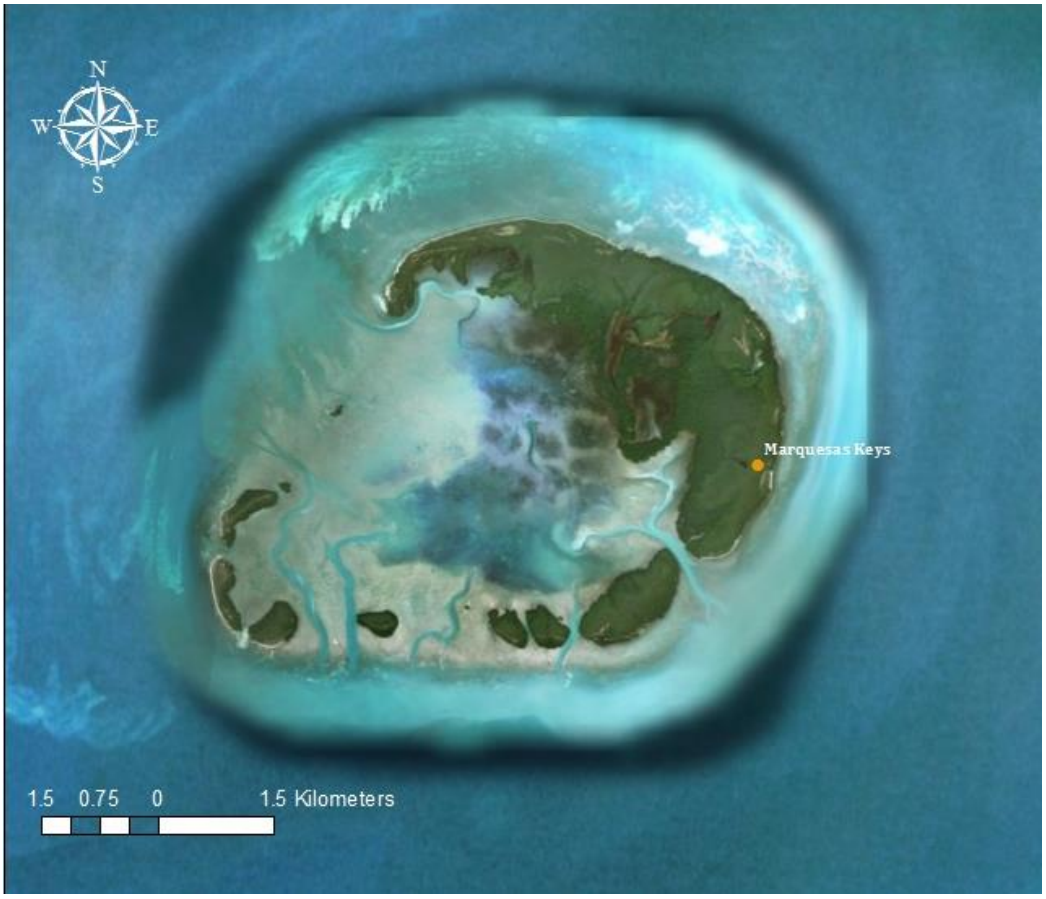

Figure 3. Satellite Map of Marquesas Keys
Coring site on Marquesas Keys (site name LK1, 210 meters from shoreline), an overwash island with a protected basin of mangrove forest and shallow seagrass meadows. Source: Esri, DigitalGlobe, GeoEye, Earthstar Geographics, CNES/Airbus DS, USDA, USGS, AeroGRID, IGN, and the GIS user community.

Figure 4. Satellite Map of Big Pine Key
Coring site of Big Pine Key (site name LK5, 15 meters from shoreline), a sparse red mangrove fringe shoreline with a salt barren basin, adjacent to urban development. Source: Esri, DigitalGlobe, GeoEye, Earthstar Geographics, CNES/Airbus DS, USDA, USGS, AeroGRID, IGN, and the GIS user community.

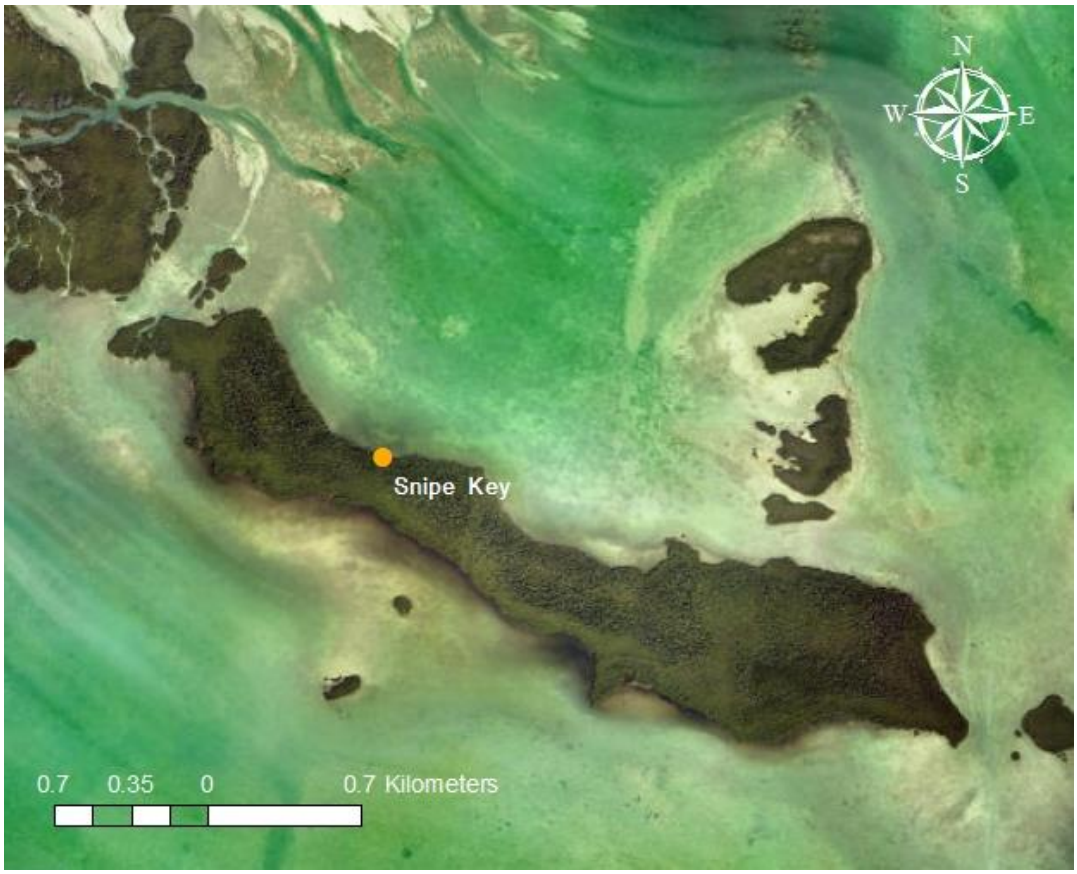

Figure 5. Satellite Map of Snipe Key
Coring site of Snipe Key (site name LK7, 15 meters from northern shoreline), a narrow island dominated by a red mangrove forest situated between channelized tidal flats. Source: Esri, DigitalGlobe, GeoEye, Earthstar Geographics, CNES/Airbus DS, USDA, USGS, AeroGRID, IGN, and the GIS user community.

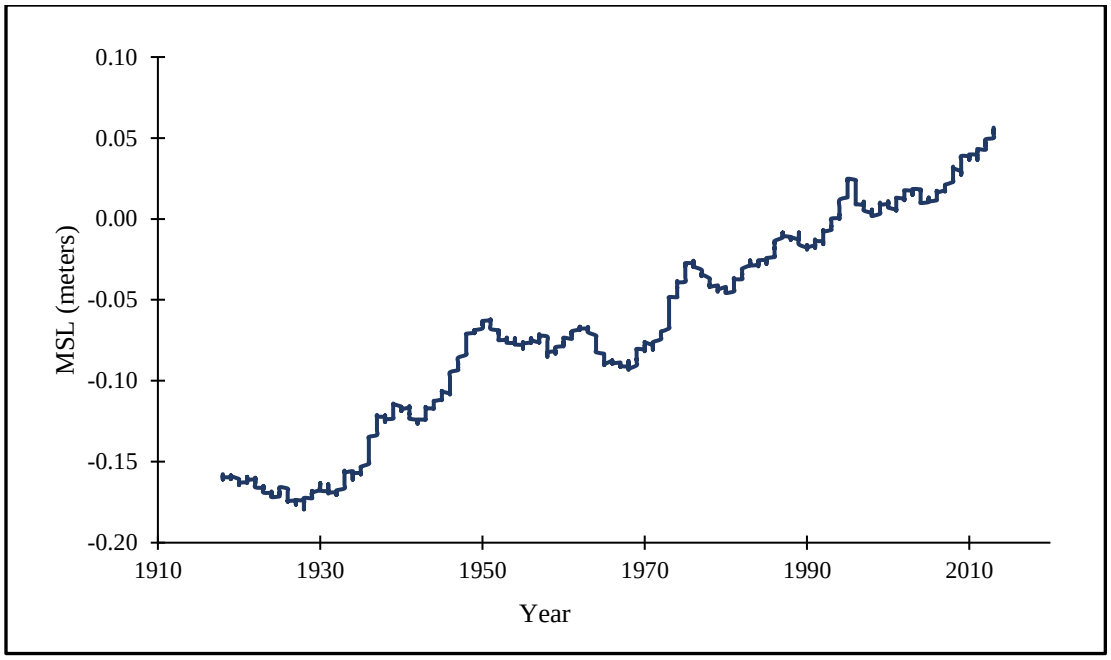

Figure 6. Key West Tidal Gauge Mean Sea Level
Five year running mean tidal gauge data from the Key West tide gauge (station ID: 8724580)

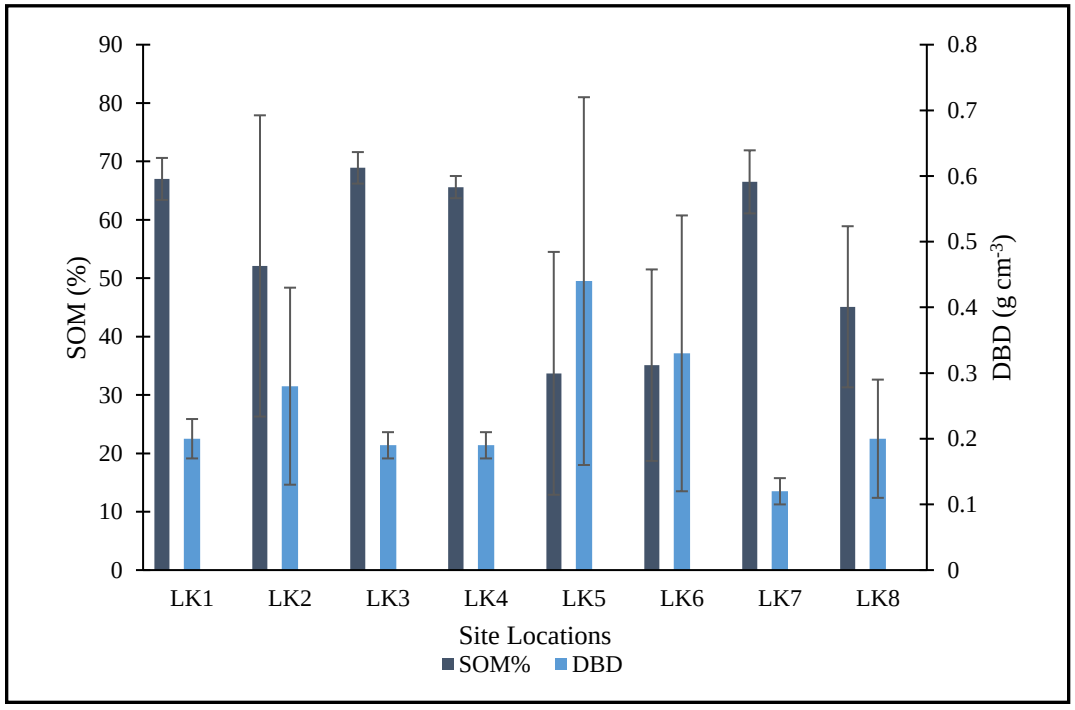

Figure 7. Soil Organic Matter and Dry Bulk Density
Comparison of dry bulk density (DBD) and soil organic matter percent (SOM%) from all cores collected during this study. Measurements were calculated from the method of loss-on-ignition (LOI).

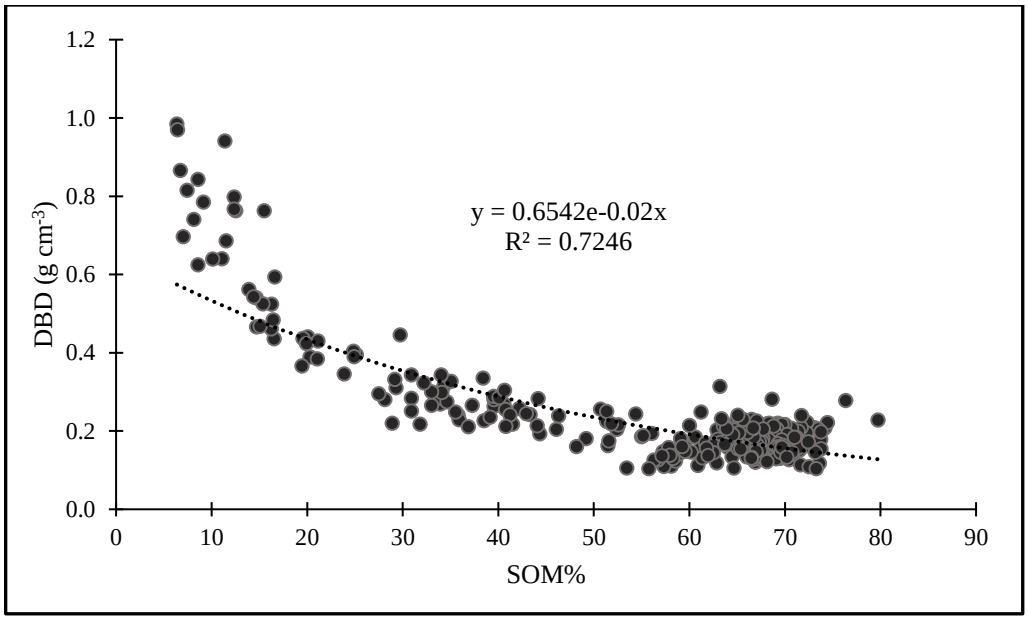

Figure 8. Exponential Regression of Soil Organic Matter and Dry Bulk Density
Negative correlation depicted by the decreasing exponential trend between soil organic matter percent (SOM%) and dry bulk density (DBD) from all sites (LK1-LK8; Table 2).

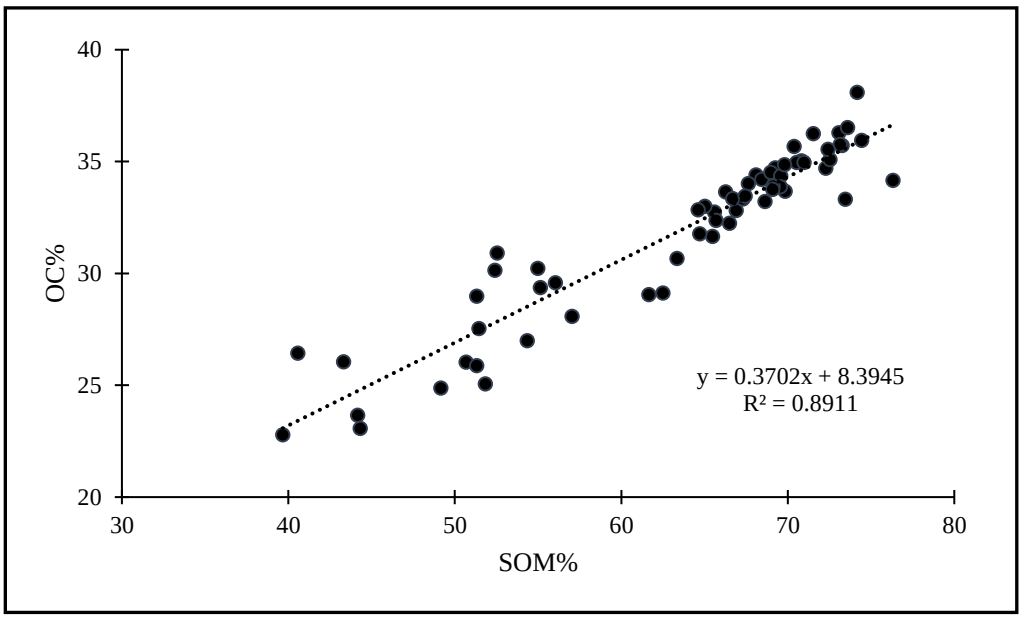

Figure 9. Linear Regression Analysis of Carbon Content and Soil Organic Matter
Soil organic matter percent (SOM%) vs organic carbon percent (OC%) across sites radiometrically dated (Marquesas Keys, Snipe Key, and Big Pine Key. SOM% obtained via loss on ignition (LOI). OC% obtained via elemental analyzer (EA). The linear regression applied allowed for a conversion factor to be made, which can be applied to region wide SOM% to get estimated OC%.

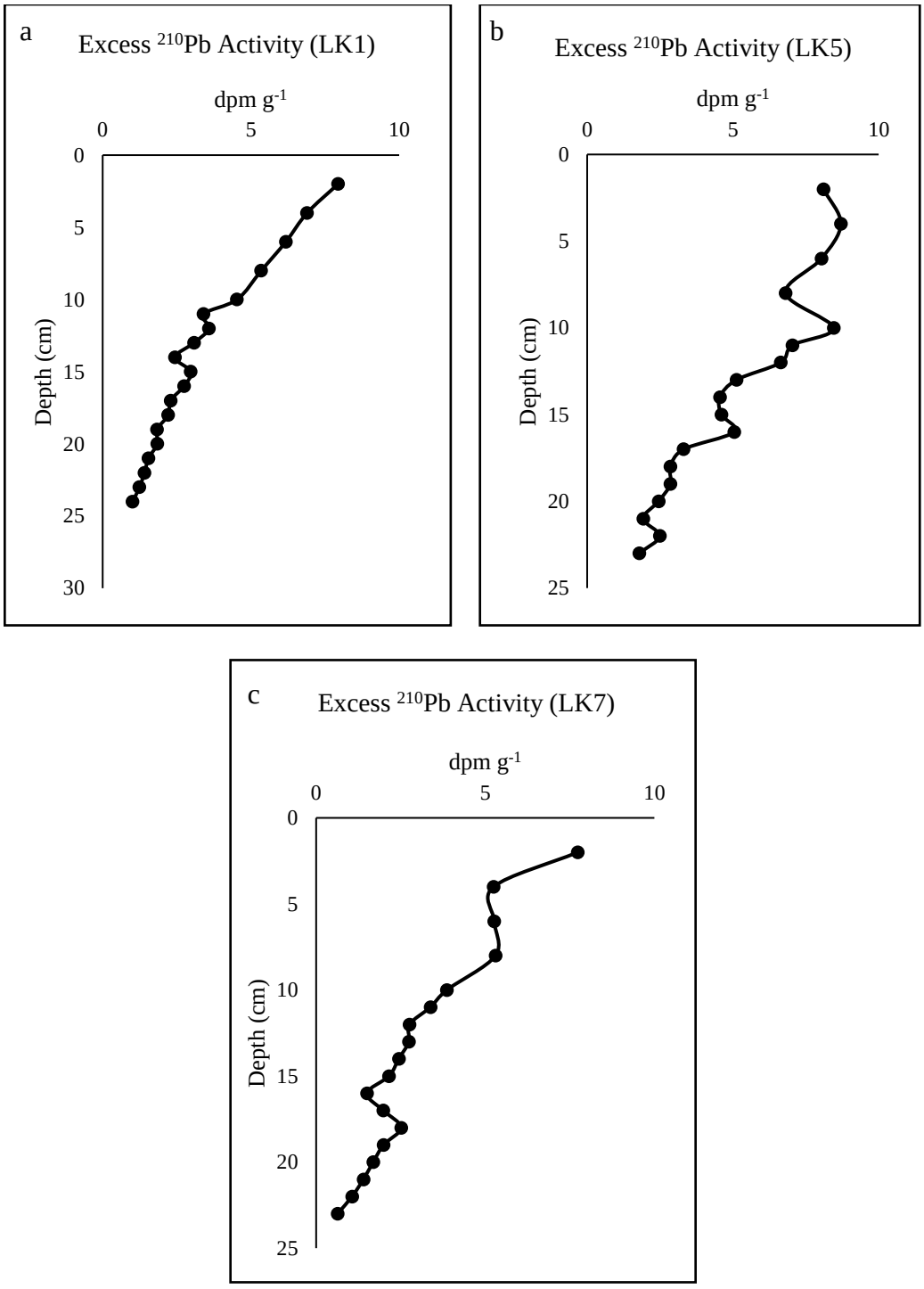

Figure 10. Excess ^{210}Lead Activity of Dated Cores
(a) Big Pine Key (LK5), (b) Marquesas Keys (LK1), (c) Snipe Key (LK7). Gamma activity was measured as counts per minute then was multiplied by a factor that includes the gamma-ray intensity and detector efficiency determined from standard calibrations allowing for conversion to disintegrations per minute (dpm g^{-1}).

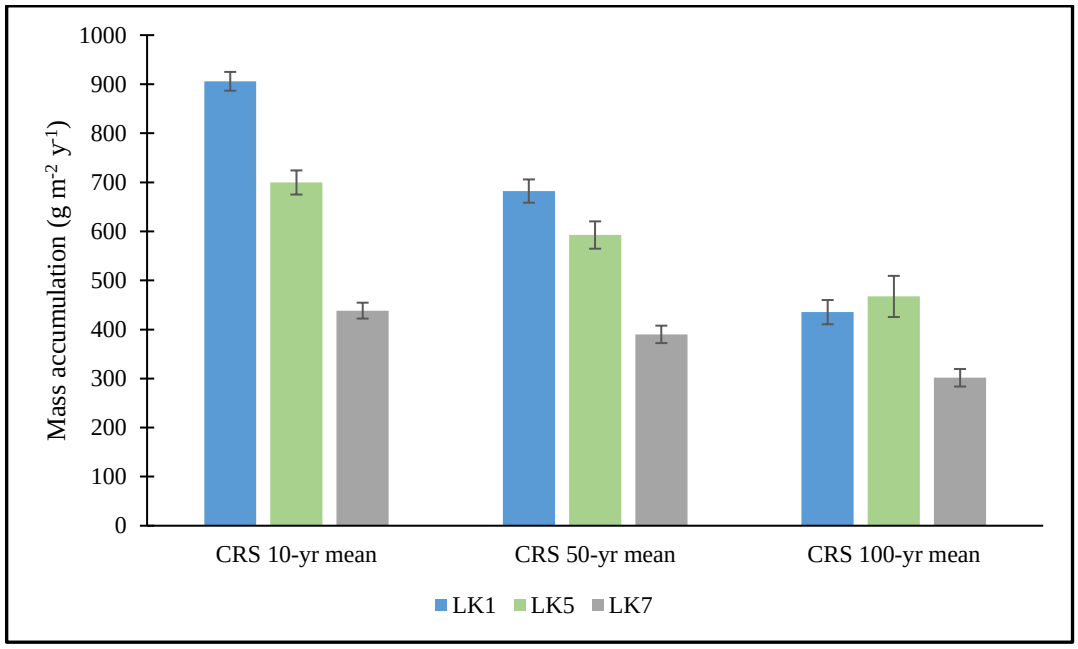

Figure 11. Graph of Mass Accumulation Rates
Mass accumulation rates (MAR) of Marquesas Keys (LK1), Big Pine Key (LK5) & Snipe Key (LK7) in 10, 50 & 100-yr most-recent means, which were found using the constant rate of supply (CRS) model via radiometric dating (^{210}Pb; centurial scale rates). Graph represents both spatial difference and timescale variability between sites.

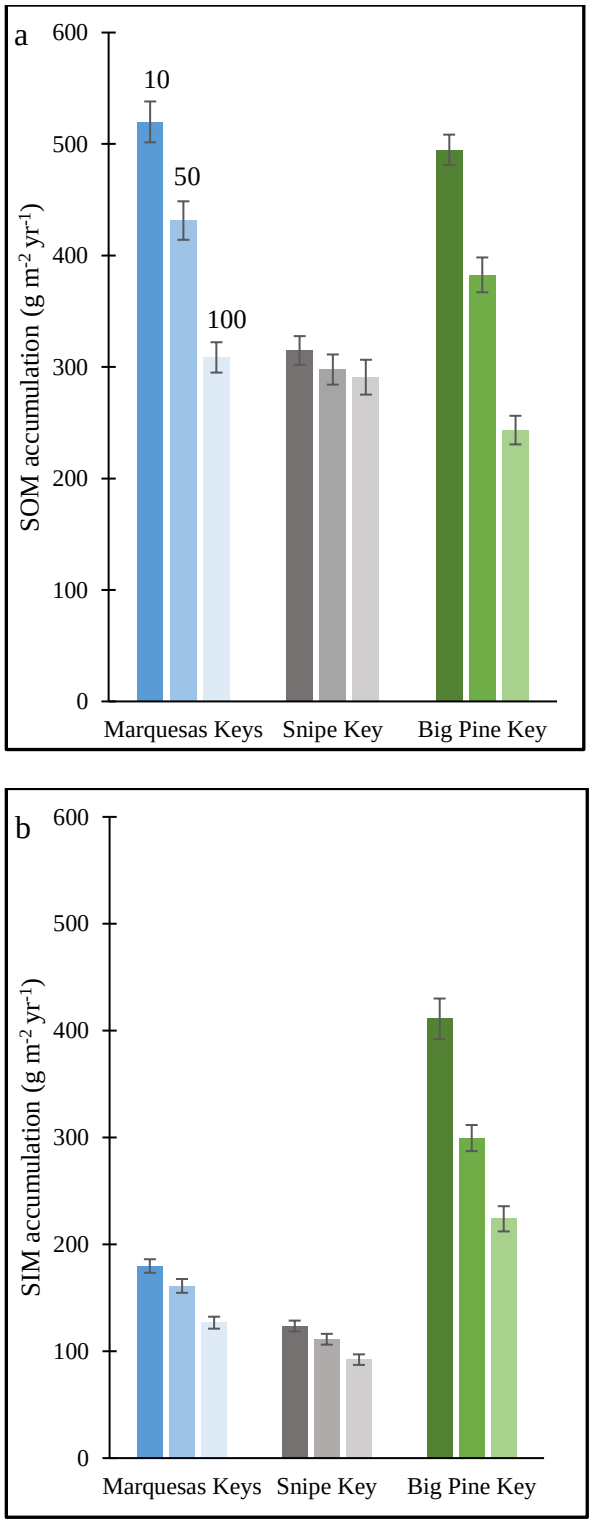

Figure 12. Soil Organic and Inorganic Matter Accumulation Rates
Soil organic matter (SOM) accumulation rates (a) & soil inorganic matter (SIM) accumulation rates (b) for Marquesas Keys (LK1), Big Pine Key (LK5) & Snipe Key (LK7). 10-, 50- & 100-yr most-recent means are displayed from dark to light shading, respectively. These means were found using the constant rate of supply (CRS) model via radiometric dating (^{210}Pb). Graphs represents both spatial difference and timescale variability between sites.

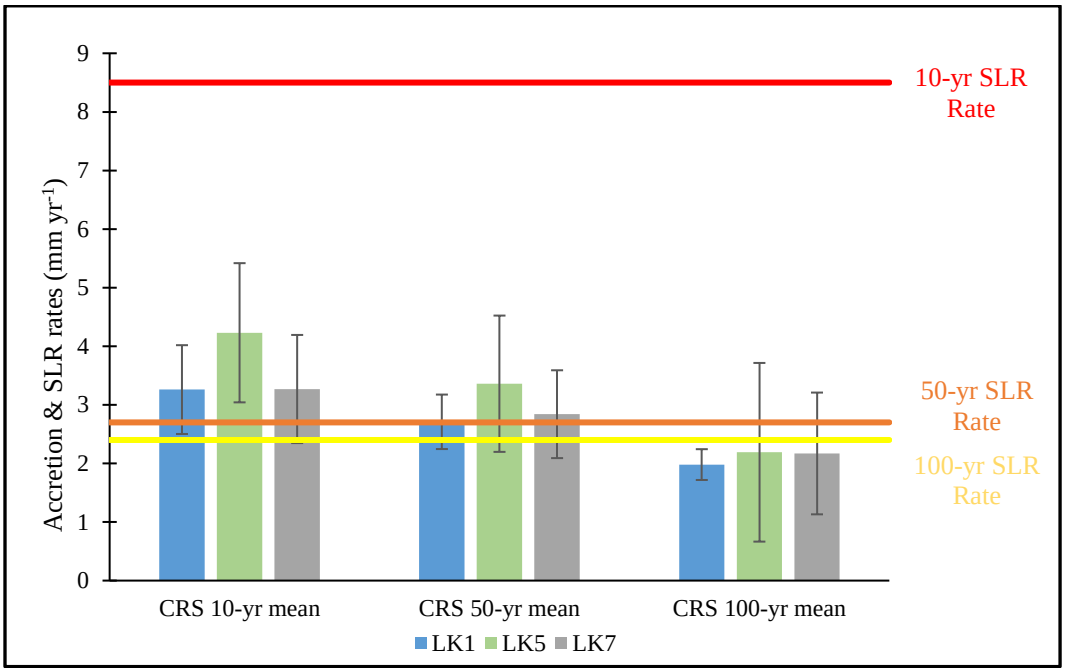

Figure 13. Accretion Rates with to Sea-Level Rise Rates Comparison
10-, 50- & 100-year most-recent mean accretion rates of Marquesas Keys (LK1), Big Pine Key (LK5) & Snipe Key (LK7) graphed against 10-, 50- & 100-year most-recent mean rates of sea-level rise (SLR). 10, 50 & 100-yr most-recent mean accretion rates were found using the constant rate of supply (CRS) model via radiometric dating (^{210}Pb; centurial scale rates).

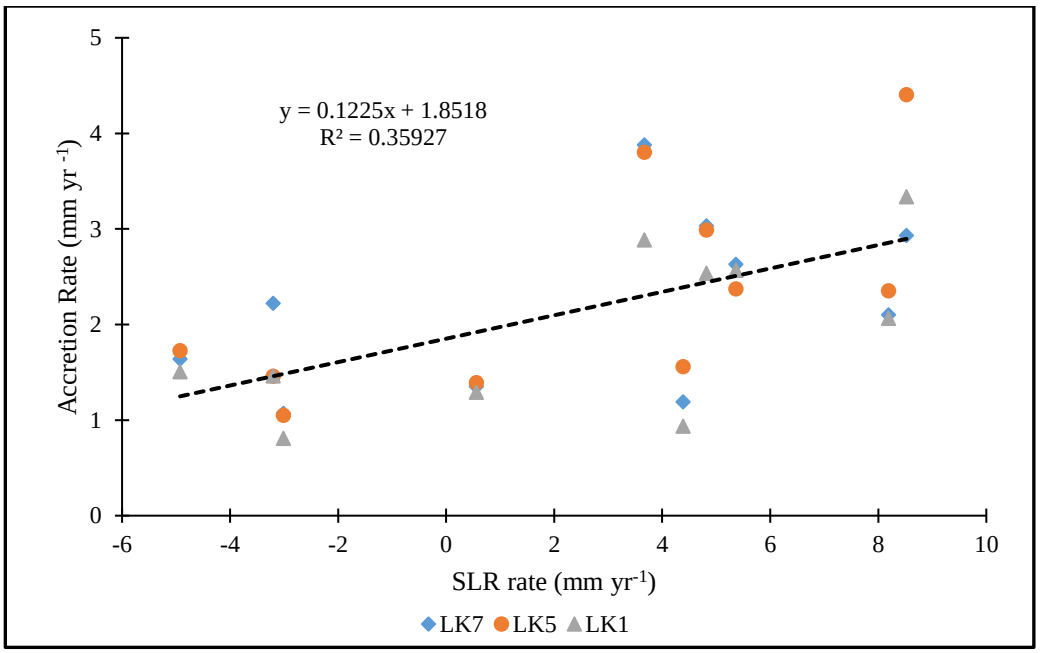

Figure 14. Plotted Accretion Rates Against Sea-Level Rise Rates
Accretion rates (Marquesas Keys, Snipe Key, and Big Pine Key) compared to sea-level rise (SLR) rates (mm yr^{-1}). Rates calculates as 10- year means from 1916 to 2015 (sampling year). The *p* value < 0.001, showing a significance in the relationship between the rates.

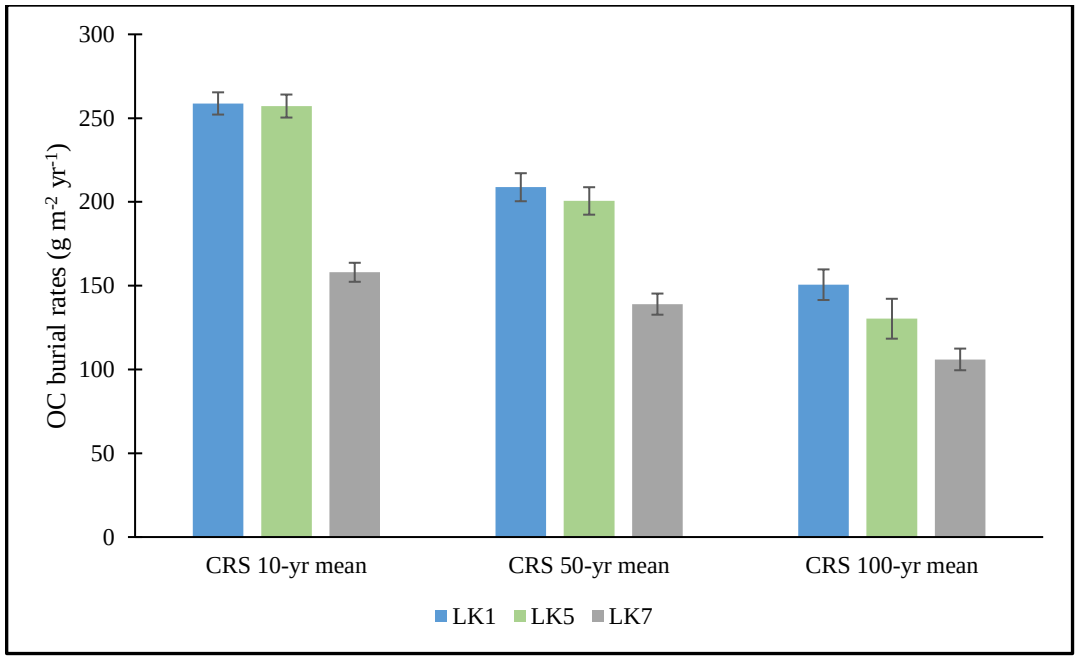

Figure 15. Organic Carbon Burial Rate
Organic carbon (OC) burial rates for Marquesas Keys (LK1), Big Pine Key (LK5) & Snipe Key (LK7). 10, 50 & 100-yr most-recent means are displayed found using the constant rate of supply (CRS) model via radiometric dating (^{210}Pb; centurial scale rates). This graph covers not only site difference but also timescale variability between them.

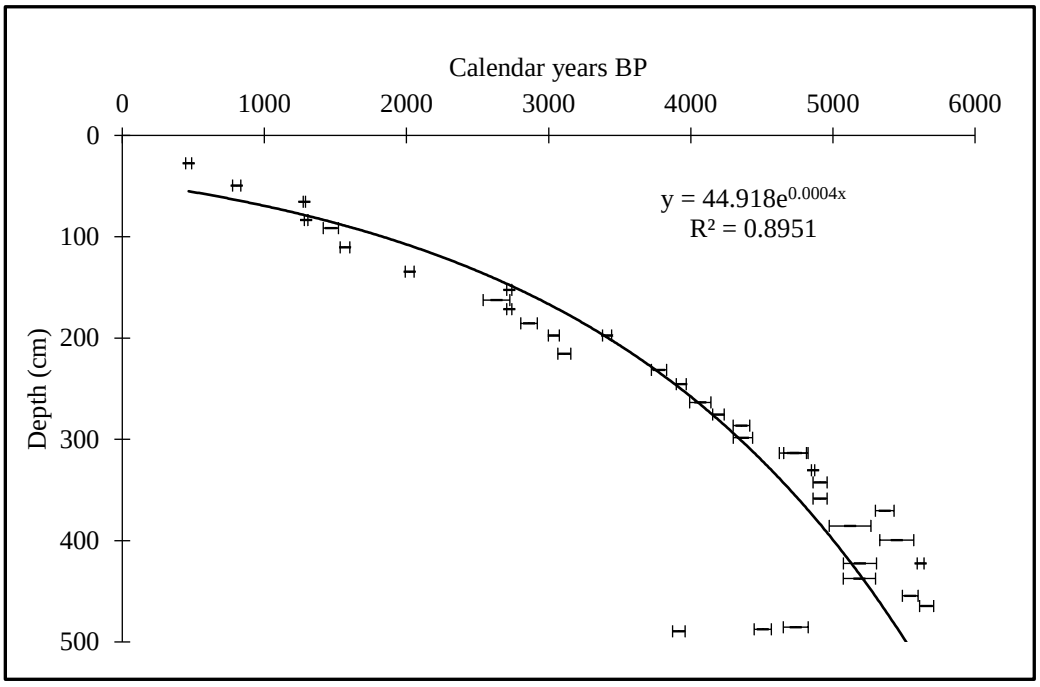

Figure 16. Radiocarbon Age-Depth Model
Radiocarbon (^{14}C) age-depth model for Snipe Key (LK7) using an exponential regression between calendar years before present (BP) and depth (cm). Horizontal error bars are ± 0.5 cm and vertical error bars are (± 1 SD) in age error.

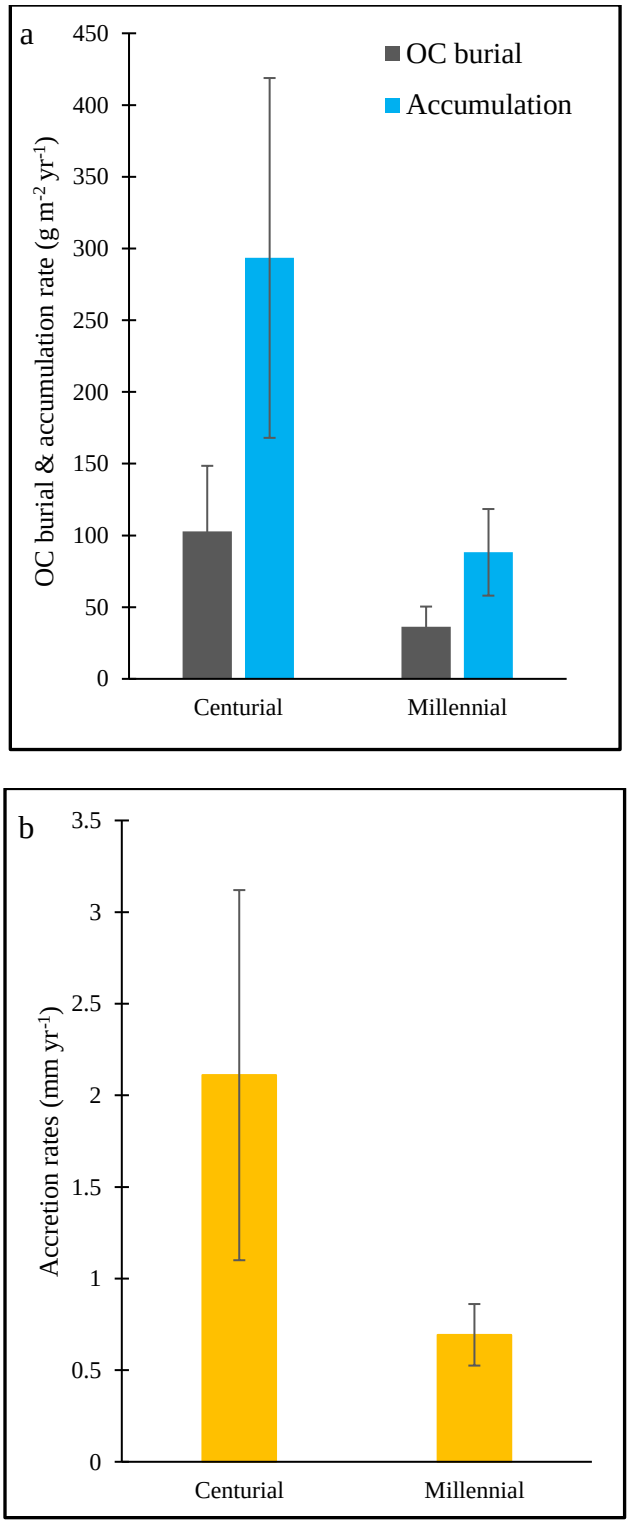

Figure 17. Centurial and Millennial Rate Comparison
Centurial and millennial rates of soil accumulation and organic carbon burial (a) and accretion (b). This rate comparison is strictly rates from Snipe Key. Centurial rates were calculated from lead-210 radiometric dating. Millennial rates were calculated from radiocarbon dating. Error bars represent standard deviation of mean values.

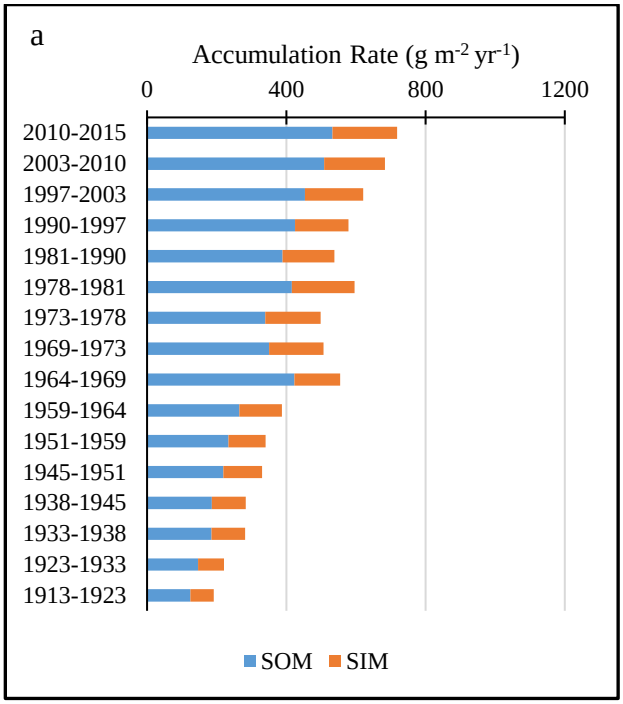
a
Accumulation Rate (g m-2 yr-1)
0
400
800
1200
2010-2015
2003-2010
1997-2003
1990-1997
1981-1990
1978-1981
1973-1978
1969-1973
1964-1969
1959-1964
1951-1959
1945-1951
1938-1945
1933-1938
1923-1933
1913-1923
SOM
SIM

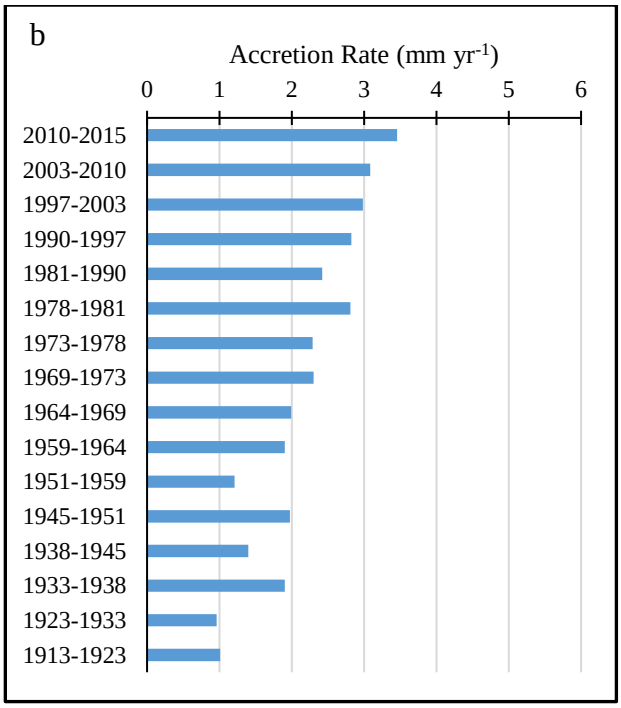
b
Accretion Rate (mm yr-1)
0
1
2
3
4
5
6
2010-2015
2003-2010
1997-2003
1990-1997
1981-1990
1978-1981
1973-1978
1969-1973
1964-1969
1959-1964
1951-1959
1945-1951
1938-1945
1933-1938
1923-1933
1913-1923

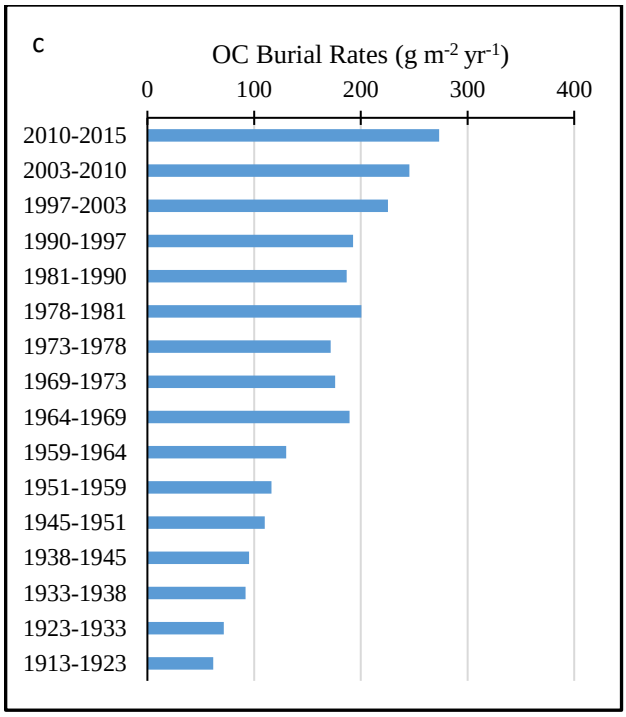

Figure 18. Marquesas Keys Age Profiles
Lead-210 CRS model dated intervals for a) soil accumulation rates, b) accretion rates, c) OC burial rates.

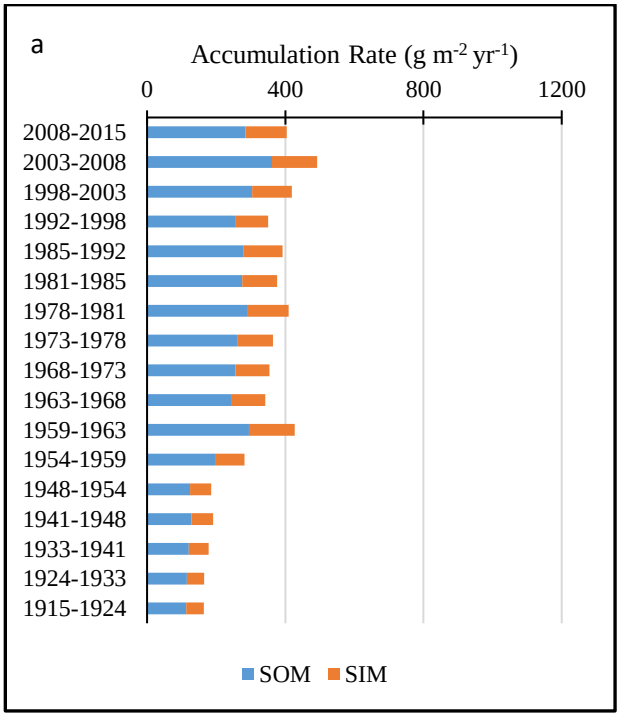

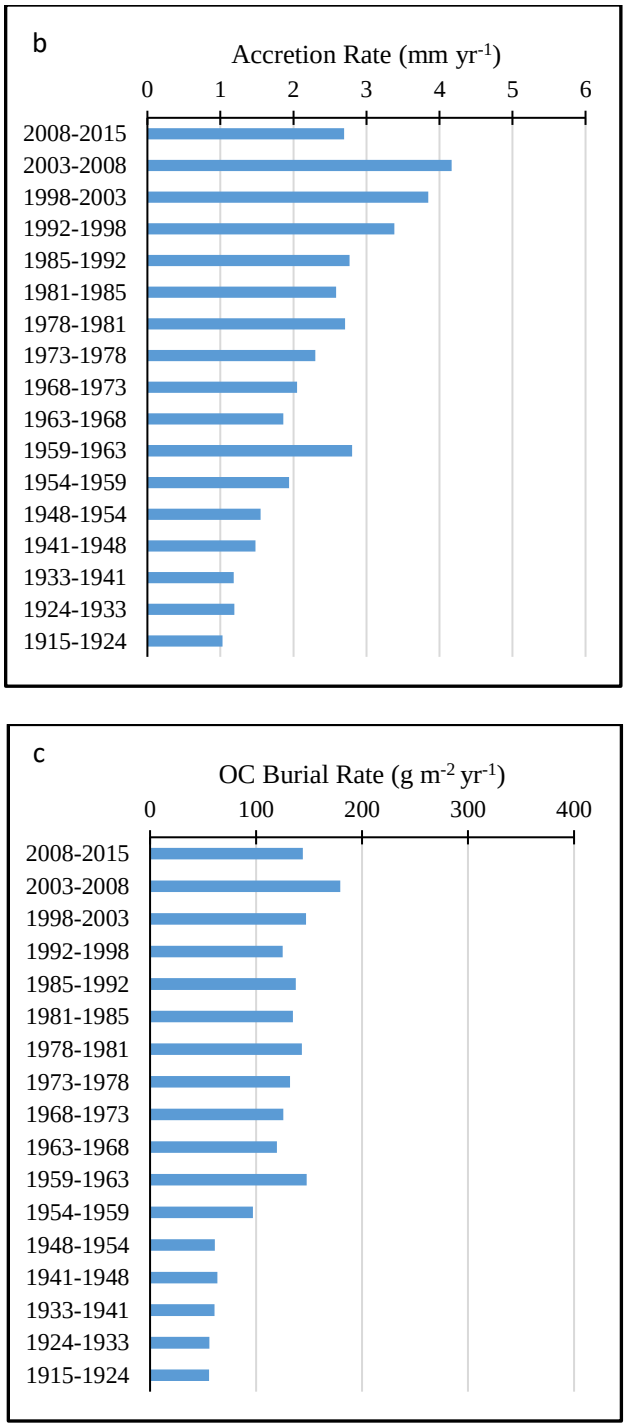

Figure 19. Snipe Key Age Profile
Lead-210 CRS model dated intervals for a) soil accumulation rates, b) accretion rates, c) OC burial rates.

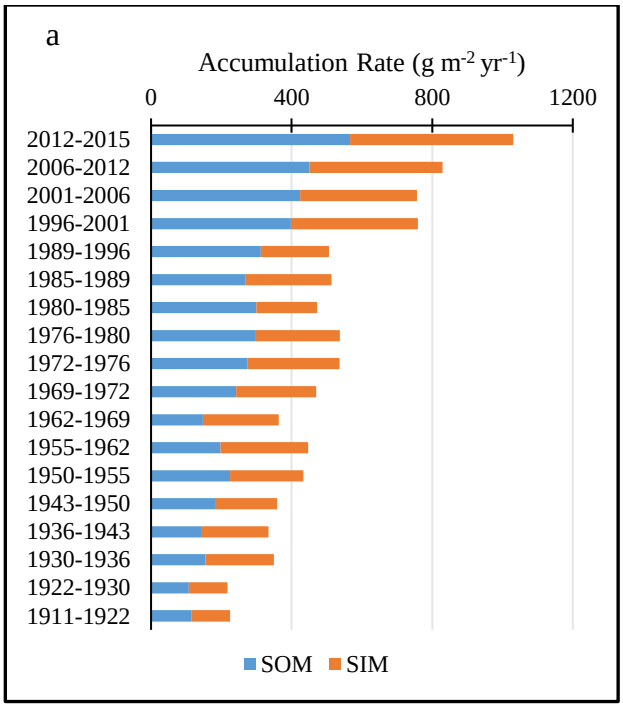
a
Accumulation Rate (g m-2 yr-1)
0
400
800
1200
2012-2015
2006-2012
2001-2006
1996-2001
1989-1996
1985-1989
1980-1985
1976-1980
1972-1976
1969-1972
1962-1969
1955-1962
1950-1955
1943-1950
1936-1943
1930-1936
1922-1930
1911-1922
SOM
SIM

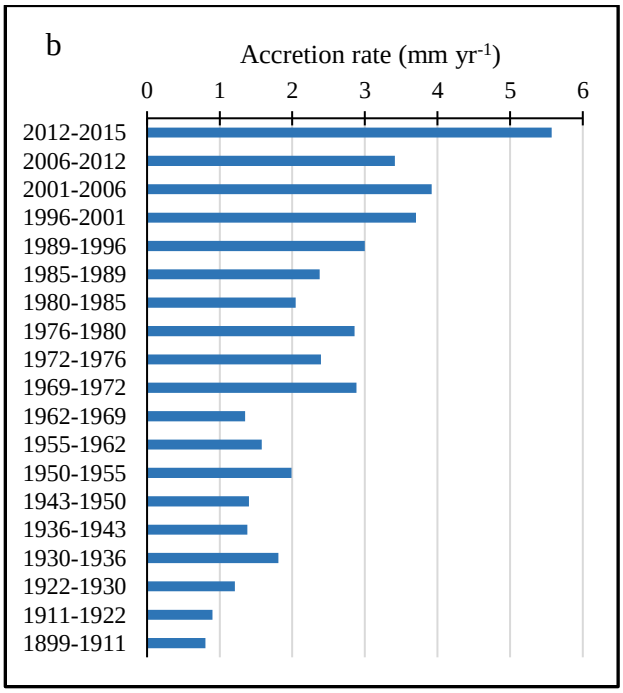
b
Accretion rate (mm yr-1)
0
1
2
3
4
5
6
2012-2015
2006-2012
2001-2006
1996-2001
1989-1996
1985-1989
1980-1985
1976-1980
1972-1976
1969-1972
1962-1969
1955-1962
1950-1955
1943-1950
1936-1943
1930-1936
1922-1930
1911-1922
1899-1911

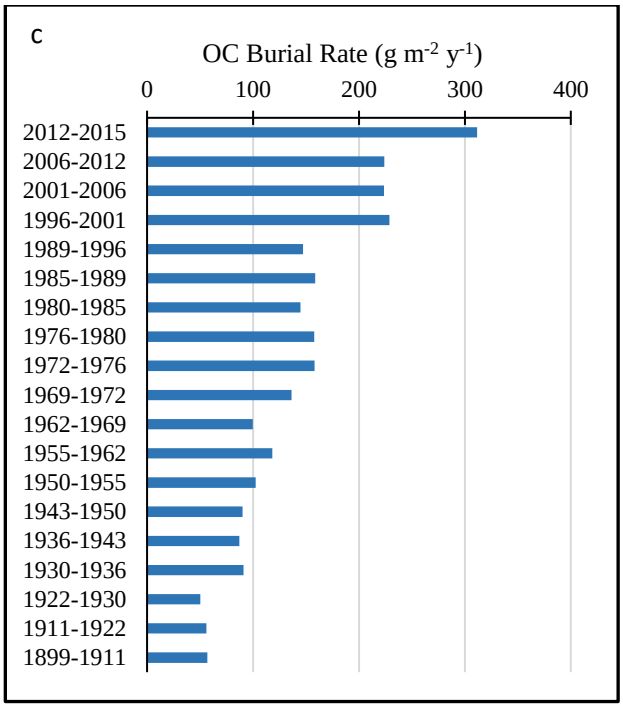

Figure 20. Big Pine Key Age Profiles
Lead-210 CRS model dated intervals for a) soil accumulation rates, b) accretion rates, c) OC burial rates.

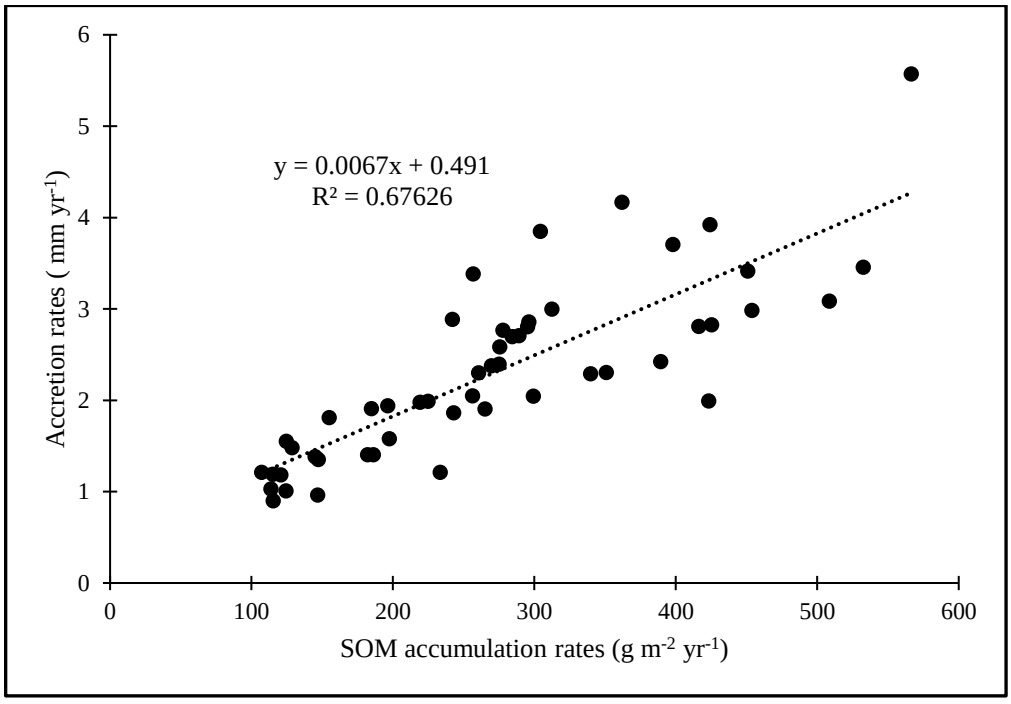

Figure 21. Accretion Rates as a Function of Soil Organic Matter Accumulation Rates
Points represent all interval depths for all sites radiometrically dated for both accretion and soil organic matter (SOM) accumulation rates.

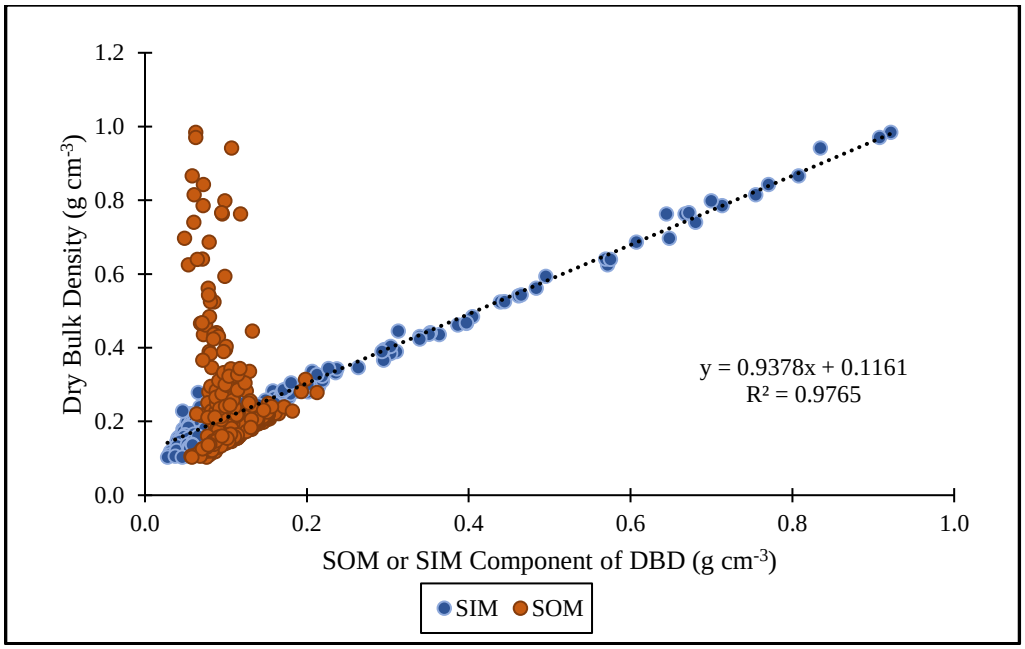

Figure 22. Soil Organic Matter and Soil Inorganic Matter Components of Dry Bulk Density
Total dry bulk density as a function of soil organic matter (SOM) & soil inorganic matter (SIM) contributing component of dry bulk density for all sites.

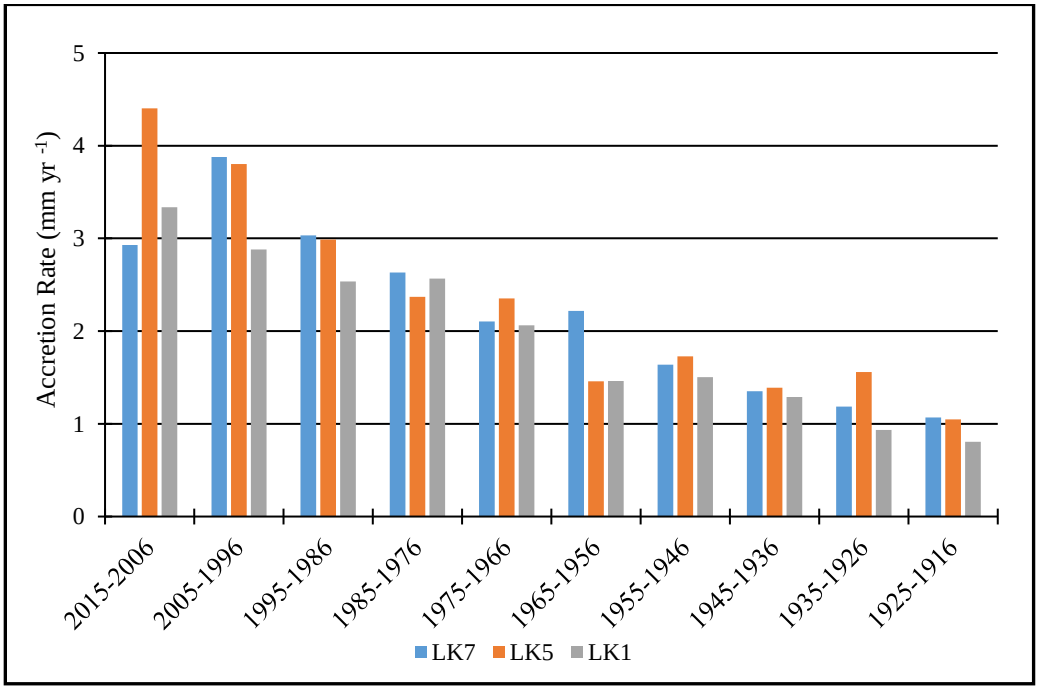

Figure 23.Ten-year Running Mean Accretion Rates
10-year means accretion rates for Marquesas Keys, Big Pine Key & Snipe Key from 1916 to 2015.

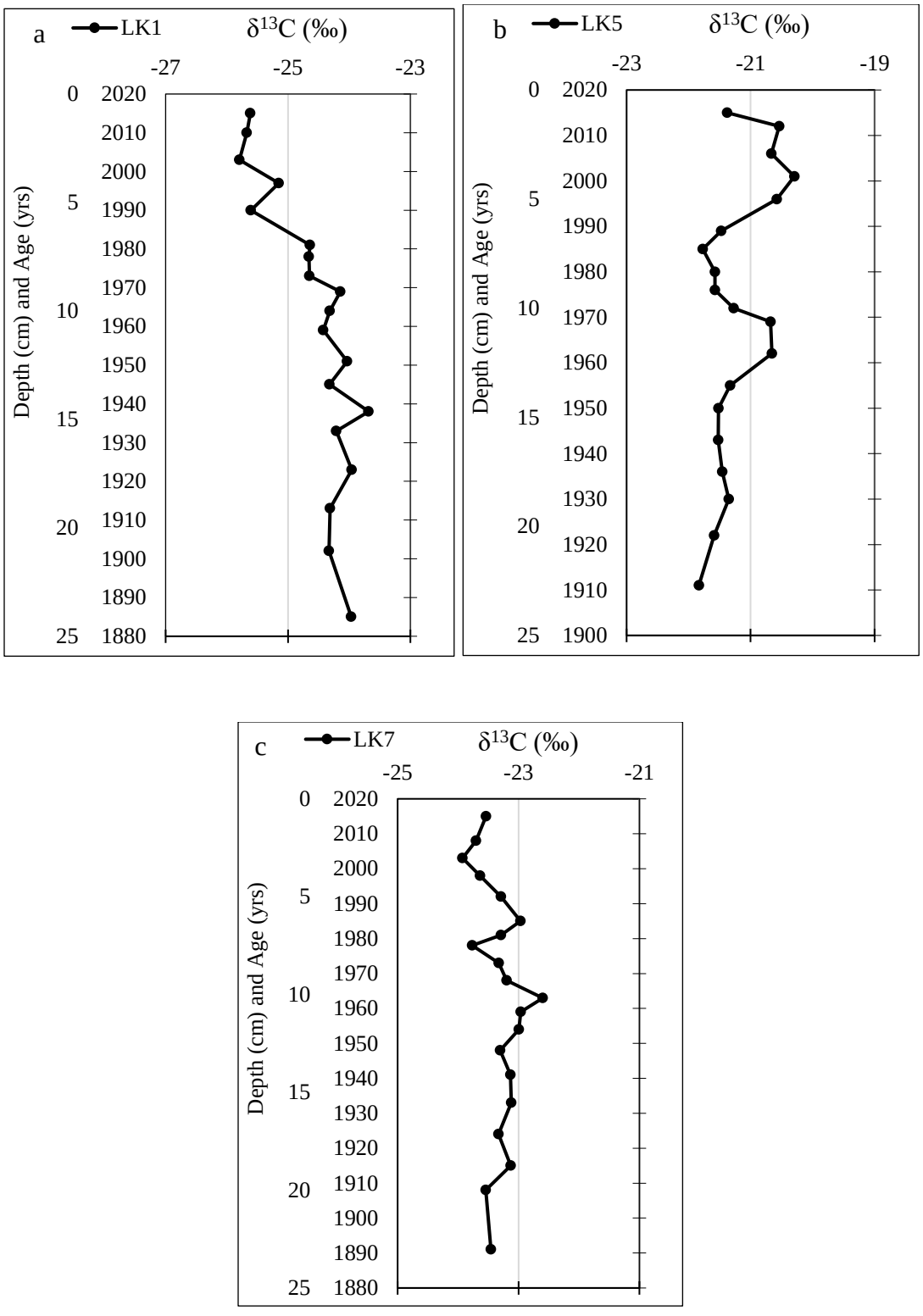

Figure 24. Stable Carbon Isotopic Ratios
$\delta^{13}C$ time series to 25 cm depth at sampling sites a) Marquesas Keys (LK1), b) Big Pine Key (LK5), and c) Snipe Key (LK7).

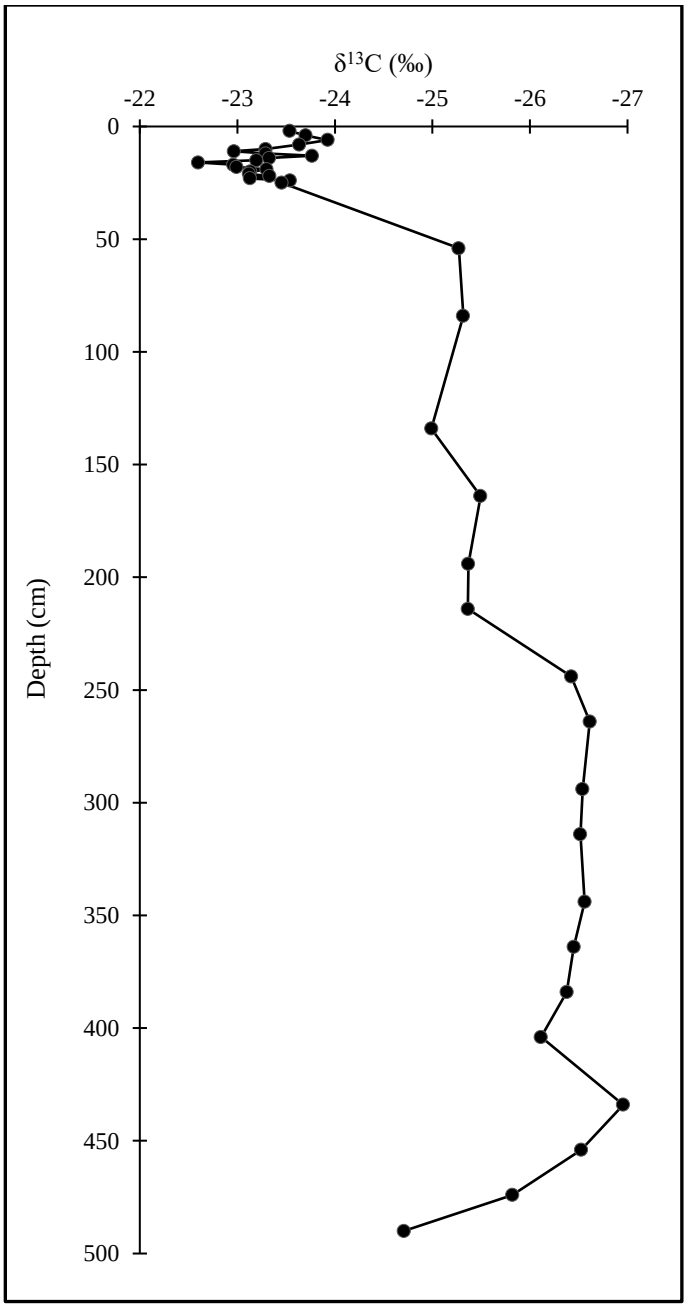

Figure 25. Stable Carbon Isotopic Ratios of Snipe Key
$\delta^{13}C$ time series to 490 cm depth the Snipe Key deep peat sequence

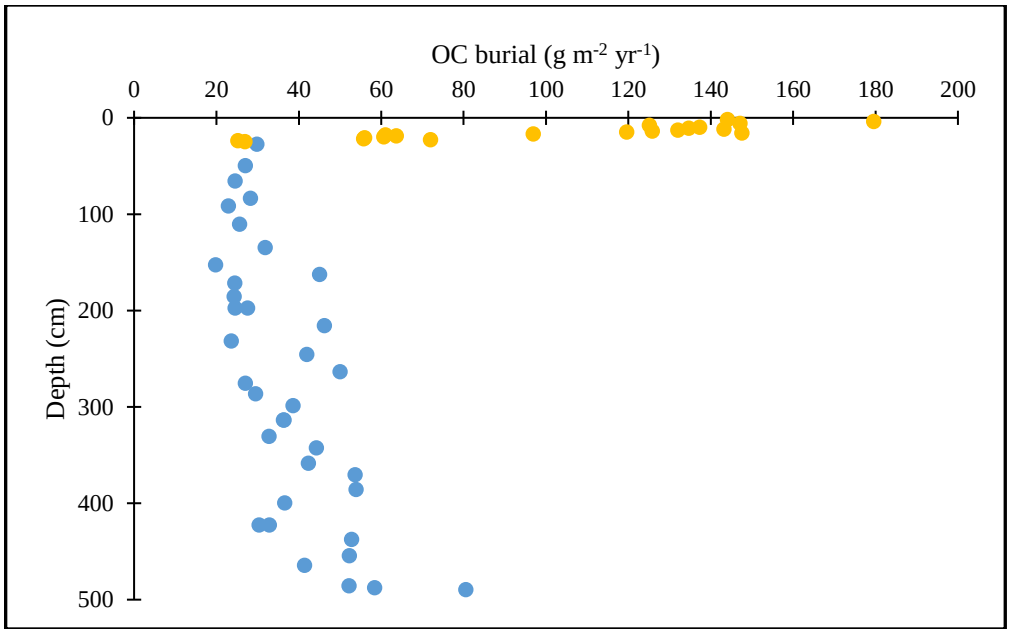

Figure 26. Comparison of ^{210}Lead and ^{14}Carbon Organic Carbon Burial Rates
Organic carbon (OC) burial rates of ^{210}Pb (yellow) and ^{14}C (blue) for depth interval dated. A common value is seen in OC burial rates around 25 cm where ^{210}Pb OC burial rates reach their maximum dateable depth and ^{14}C interval shallowest dated (27.5 cm) interval displays a similar burial rate.

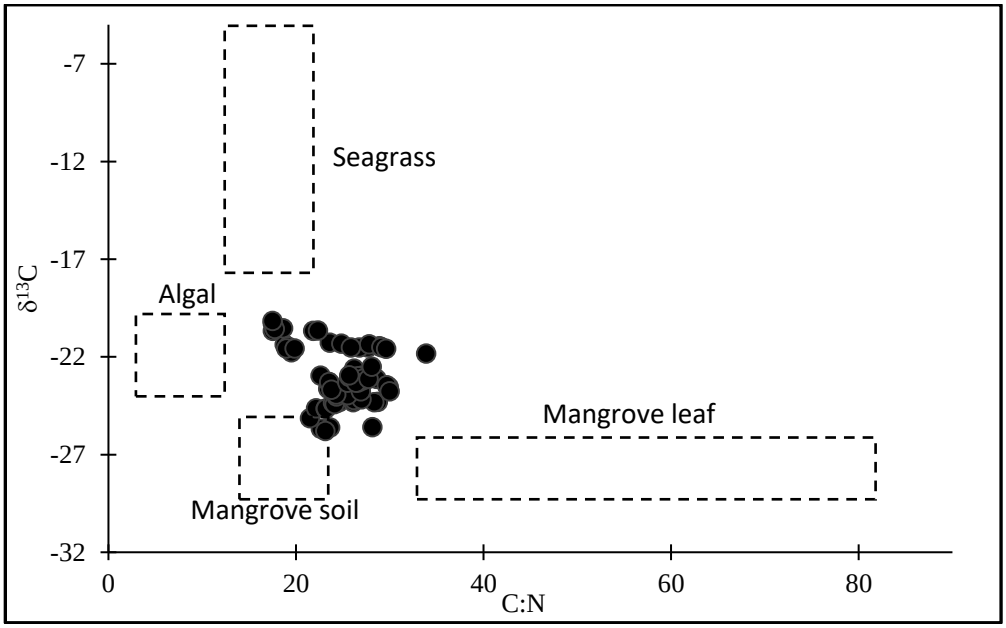

Figure 27. Stable Carbon Values Versus C:N Atomic Ratios
δ^{13}C values plotted against the ratio of organic carbon and total nitrogen. Black points represent this study's values found at Marquesas, Snipe and Big Pine Keys. The outlined squares represent range values that are possible contributing endmembers (Fry & Smith, 2002; Fourqurean & Schrlau, 2003; Gonneea et al., 2004; Campbell & Fourqurean, 2009, 2011, 2014; Belicka et al., 2012; Harmon et al., 2014).

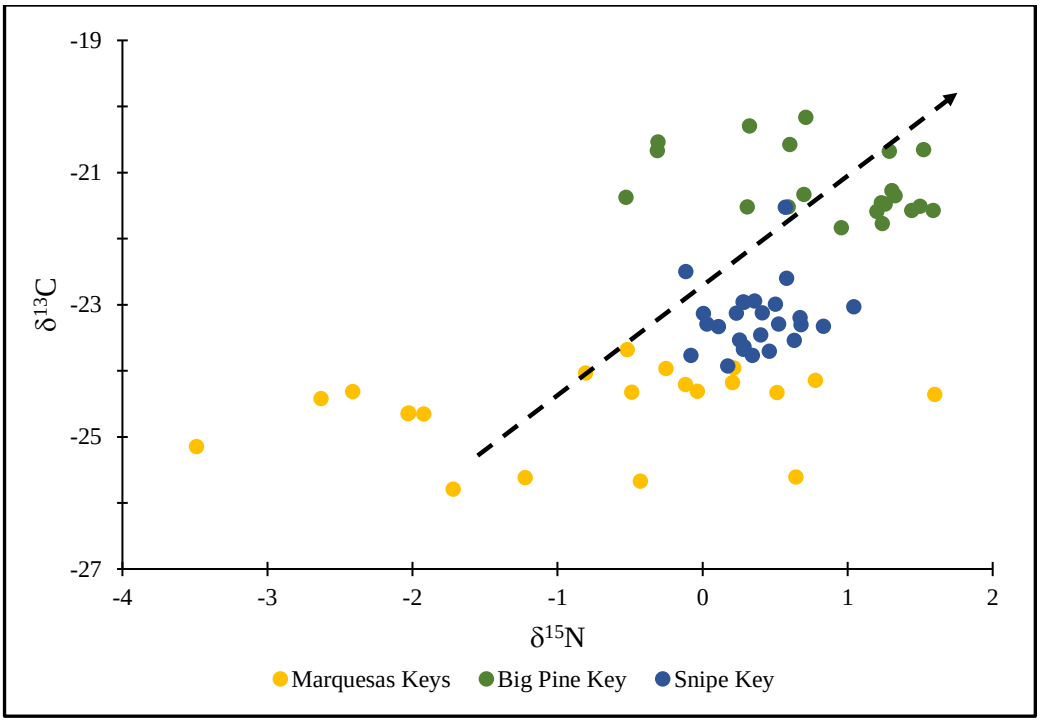

Figure 28. $\delta^{13}C$ Versus $\delta^{15}N$
Stable carbon and nitrogen ratios from three different cores collected during this study. Marquesas Keys core represents the most pristine site furthest from anthropogenic activity. Big Pine Key core represents the site closest to anthropogenic nitrogen input. The arrow represents the direction of algal and allochthonous sediment enrichment to the mangrove sediments.

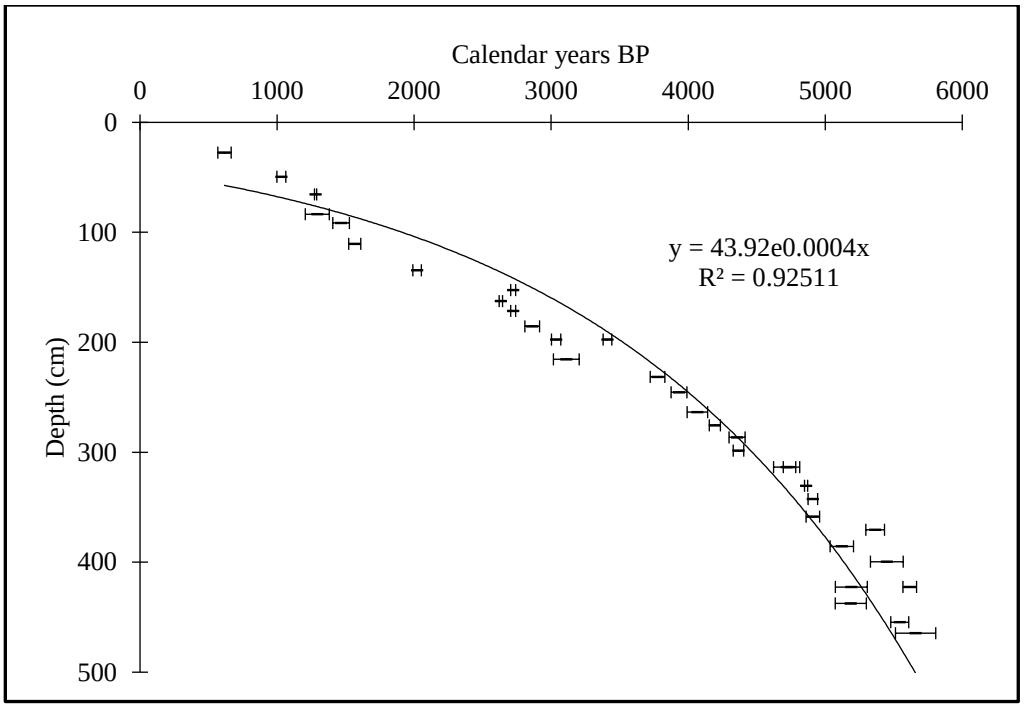

Figure 29. Adjusted Radiocarbon Age-Depth Model
Radiocarbon (^{14}C) age-depth model for Snipe Key (LK7) using an exponential regression between calendar years before present (BP) and depth (cm). Horizontal error bars are ± 0.5 cm and vertical error bars are (± 1 SD) in age error. Confounding base segments removed to improved fit.

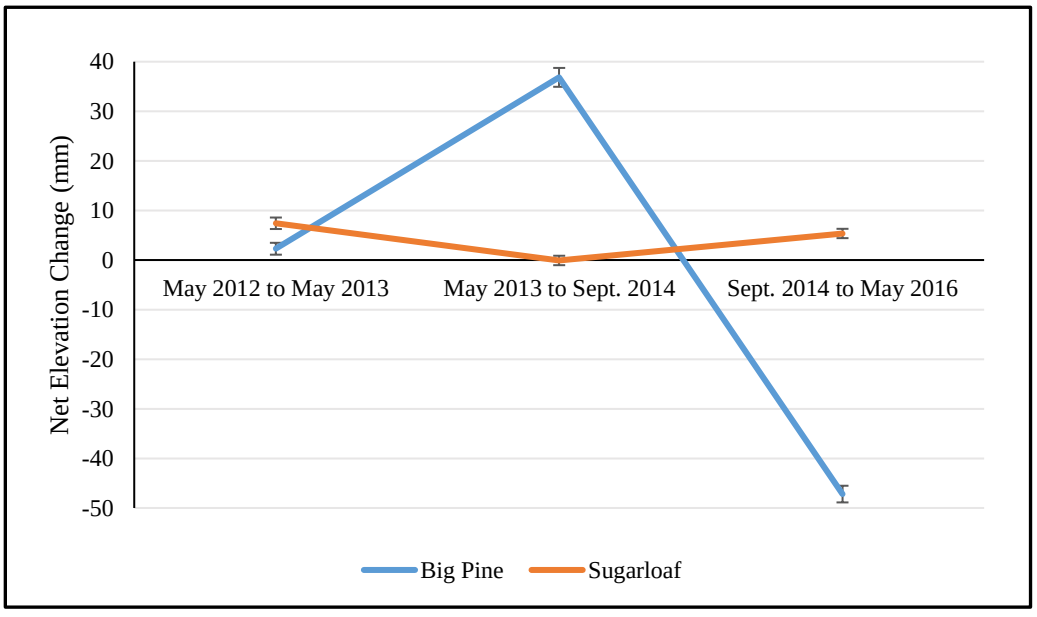

Figure 30. Net Elevation Change Measured by Surface Elevation Tables
Net elevation change measured via surface elevation tables (SET's) at Big Pine Key and Sugarloaf Key from May 2012 (date installed) to May 2016. SET's measured twice in May (2013 and 2016) and once in September (2014). No measurements were made during 2012. Error bars reported as standard error.

List of References

Adame, M. F., & Lovelock, C. E. (2011). Carbon and nutrient exchange of mangrove forests with the coastal ocean. *Hydrobiologia*, *663*(1), 23-50.

Allen, S. E., Grimshaw, H. M., Parkinson, J. A., & Quarmby, C. (1974). *Chemical analysis of ecological materials*. Blackwell Scientific Publications.

Alongi, D. M. (2014). Carbon cycling and storage in mangrove forests. *Annual review of marine science*, *6*, 195-219.

Appleby, P. G. (2001). 2001: Chronostratigraphic techniques in recent sediments. In Last, W. M and Smol, JP, editors. Tracking environmental change using lake sediments, volume 1: basin analysis, coring, and chronological techniques, Dordrecht: Kluwer Academic Publishers, 171-203.

Appleby, P. G., & Oldfield, F. (1978). The calculation of lead-210 dates assuming a constant rate of supply of unsupported 210 Pb to the sediment. *Catena*, *5*(1), 1-8.

Appleby, P. G., Nolan, P. J., Oldfield, F., Richardson, N., & Higgitt, S. R. (1988). 210 Pb dating of lake sediments and ombrotrophic peats by gamma essay. *Science of the total environment*, *69*, 157-177.

Ball, D. F. (1964). Loss-on-ignition as an estimate of organic matter and organic carbon in non-calcareous soils. *European Journal of Soil Science*, *15*(1), 84-92.

Belicka, L. L., Burkholder, D., Fourqurean, J. W., Heithaus, M. R., Macko, S. A., & Jaffé, R. (2012). Stable isotope and fatty acid biomarkers of seagrass, epiphytic, and algal organic matter to consumers in a pristine seagrass ecosystem. *Marine and Freshwater Research*, *63*(11), 1085-1097.

Bird MI, Fitfield LK, Chua S, & Goh B. (2004). Calculating sediment compaction for radiocarbon dating of intertidal sediments. Radiocarbon 46:421-435.

Bouillon, S., Connolly, R. M., & Lee, S. Y. (2008). Organic matter exchange and cycling in mangrove ecosystems: recent insights from stable isotope studies. *Journal of Sea Research*, *59*(1), 44-58.

Breithaupt, J. L., Smoak, J. M., Smith, T. J., Sanders, C. J., & Hoare, A. (2012). Organic carbon burial rates in mangrove sediments: Strengthening the global budget. *Global Biogeochemical Cycles*, *26*(3).

Breithaupt, J. L., Smoak, J. M., Smith, T. J., & Sanders, C. J. (2014). Temporal variability of carbon and nutrient burial, sediment accretion, and mass accumulation over the past century in a carbonate platform mangrove forest of the Florida Everglades. *Journal of Geophysical Research: Biogeosciences*, *119*(10), 2032-2048.

Breithaupt, J. L., Smoak, J. M., Rivera-Monroy, V. H., Castañeda-Moya, E., Moyer, R. P., Simard, M., & Sanders, C. J. (2017). Partitioning the relative contributions of organic matter and mineral sediment to accretion rates in carbonate platform mangrove soils. *Marine Geology*, *390*, 170-180.

Breithaupt, J. L., Smoak, J. M., Byrne, R. H., Waters, M. N., Moyer, R. P., & Sanders, C. J. (2018a). Avoiding timescale bias in assessments of coastal wetland vertical change. doi: 10.1002/lno.10783

Breithaupt, J. L., Smoak, J. M., Sanders, C. J., & Troxler, T. G. (2018b). Spatial Variability of Organic Carbon, CaCO 3 and Nutrient Burial Rates Spanning a Mangrove Productivity Gradient in the Coastal Everglades. *Ecosystems*, 1-15.

Cahoon, D. R., Reed, D. J., & Day Jr, J. W. (1995). Estimating shallow subsidence in microtidal salt marshes of the southeastern United States: Kaye and Barghoorn revisited. *Marine geology*, *128*(1-2), 1-9.

Cahoon, D. R., & Lynch, J. C. (1997). Vertical accretion and shallow subsidence in a mangrove forest of southwestern Florida, USA. *Mangroves and Salt Marshes*, *1*(3), 173-186.

Cahoon, D. R., & Lynch, J. C. (2010). Surface Elevation Tables. https://www.pwrc.usgs.gov/set/.

Callaway, J. C., DeLaune, R. D., & Patrick Jr, W. H. (1997). Sediment accretion rates from four coastal wetlands along the Gulf of Mexico. *Journal of Coastal Research*, 181-191.

Campbell, J. E., & Fourqurean, J. W. (2009). Interspecific variation in the elemental and stable isotope content of seagrasses in South Florida. *Marine Ecology Progress Series*, *387*, 109-123.

Campbell, J. E., & Fourqurean, J. W. (2011). Novel methodology for in situ carbon dioxide enrichment of benthic ecosystems. *Limnology and Oceanography: Methods*, *9*(3), 97-109.

Campbell, J. E., & Fourqurean, J. W. (2014). Ocean acidification outweighs nutrient effects in structuring seagrass epiphyte communities. *Journal of Ecology*, *102*(3), 730-737.

Chambers, L. G., Davis, S. E., Troxler, T., Boyer, J. N., Downey-Wall, A., & Scinto, L. J. (2014). Biogeochemical effects of simulated sea level rise on carbon loss in an Everglades mangrove peat soil. *Hydrobiologia*, *726*(1), 195-211.

Chmura, G. L., Anisfeld, S. C., Cahoon, D. R., & Lynch, J. C. (2003). Global carbon sequestration in tidal, saline wetland soils. *Global biogeochemical cycles*, *17*(4).

Choi Y, & Wang Y (2004) Dynamics of carbon sequestration in a coastal wetland using radiocarbon measurements. Global Biogeochemical Cycles. 18, GB4016. doi:10.1029/2004GB002261

Coldren, G. A., Langley, J. A., Feller, I. C., & Chapman, S. K. (2018). Warming accelerates mangrove expansion and surface elevation gain in a subtropical wetland. *Journal of Ecology*.

Coplen, T. B. (2011). Guidelines and recommended terms for expression of stable-isotope-ratio and gas-ratio measurement results. *Rapid Communications in Mass Spectrometry*, *25*(17), 2538-2560

Corbett, D. R., Burnett, W. C., & Chanton, J. P. (2017). Submarine Groundwater Discharge: An Unseen Yet Potentially Important Coastal Phenomenon. Retrieved January 24, 2018, from http://edis.ifas.ufl.edu/sg060

Corbett, D. R. & Walsh, J. P. (2015). 210lead and 137cesium. *Handbook of sea-level research*, 361-372.

Costanzo, S. D., Udy, J., Longstaff, B., & Jones, A. (2005). Using nitrogen stable isotope ratios (δ15N) of macroalgae to determine the effectiveness of sewage upgrades: changes in the extent of sewage plumes over four years in Moreton Bay, Australia. *Marine Pollution Bulletin*, *51*(1-4), 212-217.

Craft, C. B., Seneca, E. D., & Broome, S. W. (1991). Loss on ignition and Kjeldahl digestion for estimating organic carbon and total nitrogen in estuarine marsh soils: calibration with dry combustion. *Estuaries*, *14*(2), 175-179.

Davies, B. E. (1974). Loss-on-ignition as an estimate of soil organic matter 1. *Soil Science Society of American Journal, 38* (1), 150-151.

Dean, W.E. (1974). Determination of carbonate and organic matter in calcareous sediments and sedimentary rocks by loss on ignition: Comparison with other methods. Journal of Sedimentary Petrology 44: 242–248.

Dittmar, T., Hertkorn, N., Kattner, G., & Lara, R. J. (2006). Mangroves, a major source of dissolved organic carbon to the oceans. *Global biogeochemical cycles*, *20*(1).

Donato DC, Kauffman JB, Murdiyarso D, Kurnianto S, Stidham M, Kanninen M. (2011). Mangroves among the most carbon-rich forests in the tropics. *Nat. Geosci.* 4:293–97.

Doyle, T. W., Krauss, K. W., Conner, W. H., & From, A. S. (2010). Predicting the retreat and migration of tidal forests along the northern Gulf of Mexico under sea-level rise. *Forest Ecology and Management*, *259*(4), 770-777.

Drexler JZ, & Ewel KC. (2001). Effect of the 1997–1998 ENSO-related drought on hydrology and salinity in a Micronesian wetland complex. Estuaries 24: 347–356.

Duarte, C. M., Middelburg, J. J., & Caraco, N. F. (2005). Major role of marine vegetation on the oceanic carbon cycle. *Biogeosciences*, *2*(1), 1-8.

Ehleringer, J. R., Buchmann, N., & Flanagan, L. B. (2000). Carbon isotope ratios in belowground carbon cycle processes. *Ecological Applications*, *10*(2), 412-422.

Farnsworth EJ, Ellison AM, & Gong WK. (1996). Elevated CO_2 alters anatomy, physiology, growth, and reproduction of red mangrove (Rhizophora mangle L.). Oecologia 108: 599–609.

Fontaine, S., & Barot, S. (2005). Size and functional diversity of microbe populations control plant persistence and long-term soil carbon accumulation. *Ecology Letters*, *8*(10), 1075-1087.

Fourqurean, J. W., & Schrlau, J. E. (2003). Changes in nutrient content and stable isotope ratios of C and N during decomposition of seagrasses and mangrove leaves along a nutrient availability gradient in Florida Bay, USA. *Chemistry and Ecology*, *19*(5),

373-390.

Fourqurean, J. W., Zieman, J. C., & Powell, G. V. (1992). Phosphorus limitation of primary production in Florida Bay: evidence from C: N: P ratios of the dominant seagrass Thalassia testudinum. *Limnology and Oceanography*, *37*(1), 162-171.

Fry, B., Bern, A. L., Ross, M. S., & Meeder, J. F. (2000). δ15N studies of nitrogen use by the red mangrove, Rhizophora mangle L. in south Florida. *Estuarine, Coastal and Shelf Science*, *50*(2), 291-296.

Fry, B., & Smith, T. J. (2002). Stable isotope studies of red mangroves and filter feeders from the Shark River estuary, Florida. *Bulletin of Marine Science*, *70*(3), 871-890.

Furukawa K, Wolanski E, Mueller H. (1997). Currents and sediment transport in mangrove forests. Estuarine, Coastal and Shelf Science 44: 301–310.

Gäggeler, H., Von Gunten, H. R., & Nyffeler, U. (1976). Determination of 210Pb in lake sediments and in air samples by direct gamma-ray measurement. *Earth and Planetary Science Letters*, *33*(1), 119-121.

Gilman, E., Ellison, J., & Coleman, R. (2007). Assessment of mangrove response to projected relative sea-level rise and recent historical reconstruction of shoreline position. *Environmental monitoring and assessment*, *124*(1-3), 105-130.

Gilman EL, Ellison JC, Duke NC, & Field C. (2008). Threats to mangroves from climate change and adaptation options: a review. Aquatic Botany 89: 237–250.

Giri, C., Ochieng, E., Tieszen, L. L., Zhu, Z., Singh, A., Loveland, T., ... & Duke, N. (2011). Status and distribution of mangrove forests of the world using earth observation satellite data. *Global Ecology and Biogeography*, *20*(1), 154-159.

Gonneea, M. E., Paytan, A., & Herrera-Silveira, J. A. (2004). Tracing organic matter sources and carbon burial in mangrove sediments over the past 160 years. *Estuarine, Coastal and Shelf Science*, *61*(2), 211-227.

Harmon, T. S., Smoak, J. M., Waters, M. N., & Sanders, C. J. (2014). Hydrologic fragmentation-induced eutrophication in Dove Sound, Upper Florida Keys, USA. *Environmental Earth Sciences*, *71*(10), 4387-4395.

Hine, A. C. (2013). Geologic history of Florida: major events that formed the Sunshine State.

Holguin, G., Vazquez, P., & Bashan, Y. (2001). The role of sediment microorganisms in the productivity, conservation, and rehabilitation of mangrove ecosystems: an overview. *Biology and fertility of soils*, *33*(4), 265-278.

Hsu, H., & Lachenbruch, P. A. (2008). Paired t test. *Wiley Encyclopedia of Clinical Trials*.

IPCC, 2013: Summary for Policymakers. In: Climate Change 2013: The Physical Science Basis. Contribution of Working Group I to the Fifth Assessment Report of the Intergovernmental Panel on Climate Change [Stocker, T.F., D. Qin, G.-K. Plattner, M. Tignor, S.K. Allen, J. Boschung, A. Nauels, Y. Xia, V. Bex and P.M. Midgley (eds.)]. Cambridge University Press, Cambridge, United Kingdom and New York, NY, USA.

Jennerjahn, T. C., & Ittekkot, V. (2002). Relevance of mangroves for the production and deposition of organic matter along tropical continental margins. *Naturwissenschaften*, *89*(1), 23-30.

Kauffman, J.B. and Donato, D.C. (2012). Protocols for the measurement, monitoring and reporting of structure, biomass and carbon stocks in mangrove forests. Working Paper 86. CIFOR, Bogor, Indonesia.

Kaye, C. A., & Barghoorn, E. S. (1964). Late Quaternary sea-level change and crustal rise at Boston, Massachusetts, with notes on the autocompaction of peat. *Geological Society of America Bulletin*, *75*(2), 63-80.

Kemmitt, S. J., Lanyon, C. V., Waite, I. S., Wen, Q., Addiscott, T. M., Bird, N. R., ... & Brookes, P. C. (2008). Mineralization of native soil organic matter is not regulated by the size, activity or composition of the soil microbial biomass—a new perspective. *Soil Biology and Biochemistry*, *40*(1), 61-73.

Khan, N. S., Ashe, E., Horton, B. P., Dutton, A., Kopp, R. E., Brocard, G., ... & Scatena, F. N. (2017). Drivers of Holocene sea-level change in the Caribbean. *Quaternary Science Reviews*, *155*, 13-36.

Kirwan, M. L., & Megonigal, J. P. (2013). Tidal wetland stability in the face of human impacts and sea-level rise. *Nature*, *504*(7478), 53.

Koch, M. S., & Snedaker, S. C. (1997). Factors influencing Rhizophora mangle L. seedling development in Everglades carbonate soils. *Aquatic Botany*, *59*(1-2), 87-98.

Krauss, K. W., McKee, K. L., Lovelock, C. E., Cahoon, D. R., Saintilan, N., Reef, R., & Chen, L. (2014). How mangrove forests adjust to rising sea level. *New phytologist*, *202*(1), 19-34.

Kristensen, E., Bouillon, S., Dittmar, T., & Marchand, C. (2008). Organic carbon dynamics in mangrove ecosystems: a review. *Aquatic Botany*, *89*(2), 201-219.

Ku, T. C. W., Walter, L. M., Coleman, M. L., Blake, R. E., & Martini, A. M. (1999). Coupling between sulfur recycling and syndepositional carbonate dissolution: evidence from oxygen and sulfur isotope composition of pore water sulfate, South Florida Platform, USA. *Geochimica et Cosmochimica Acta*, *63*(17), 2529-2546.

Lallier-Verges, E., Perrussel, B. P., Disnar, J. R., & Baltzer, F. (1998). Relationships between environmental conditions and the diagenetic evolution of organic matter derived from higher plants in a modern mangrove swamp system (Guadeloupe, French West Indies). *Organic Geochemistry*, *29*(5-7), 1663-1686.

Lapointe, B. E., Barile, P. J., & Matzie, W. R. (2004). Anthropogenic nutrient enrichment of seagrass and coral reef communities in the Lower Florida Keys: discrimination of local versus regional nitrogen sources. *Journal of Experimental Marine Biology and Ecology*, *308*(1), 23-58.

Lazo, D. E., Dyer, L. G., & Alorro, R. D. (2017). Silicate, phosphate and carbonate mineral dissolution behaviour in the presence of organic acids: A review. *Minerals Engineering*, *100*, 115-123.

Lehmann, M. F., Bernasconi, S. M., Barbieri, A., & McKenzie, J. A. (2002). Preservation of organic matter and alteration of its carbon and nitrogen isotope composition during simulated and in situ early sedimentary diagenesis. *Geochimica et Cosmochimica Acta*, *66*(20), 3573-3584.

Lin, G., & da SL Sternberg, L. (1992). Differences in morphology, carbon isotope ratios, and photosynthesis between scrub and fringe mangroves in Florida, USA. *Aquatic Botany*, *42*(4), 303-313.

Lovelock CE, Feller IC, Adame MF, Reef R, Penrose HM, Wei L, & Ball MC. (2011). Intense storms and the delivery of materials that relieve nutrient limitations in mangroves of an arid zone estuary. Functional Plant Biology 38: 514–522.

Lynch, J. C., Meriwether, J. R., McKee, B. A., Vera-Herrera, F., & Twilley, R. R. (1989). Recent accretion in mangrove ecosystems based on137Cs and210Pb. *Estuaries*, *12*(4), 284-299.

Macamo, C. C. F., Massuanganhe, E., Nicolau, D. K., Bandeira, S. O., & Adams, J. B. (2016). Mangrove's response to cyclone Eline (2000): What is happening 14 years later. *Aquatic Botany*, *134*, 10-17.

Macintyre, I. G., Toscano, M. A., & Bond, G. B. (2004). Holocene history of the mangrove islands of Twin Cays, Belize, Central America.cht

Maher, D. T., Santos, I. R., Golsby-Smith, L., Gleeson, J., & Eyre, B. D. (2013). Groundwater-derived dissolved inorganic and organic carbon exports from a mangrove tidal creek: The missing mangrove carbon sink?. *Limnology and Oceanography*, *58*(2), 475-488.

Mariotti, A., & Balesdent, J. (1990). 13C natural abundance as a tracer of soil organic matter turnover and palaeoenvironment dynamics. *Chemical Geology*, *84*(1/4), 217-219.

Marschner, B., & Kalbitz, K. (2003). Controls of bioavailability and biodegradability of dissolved organic matter in soils. *Geoderma*, *113*(3-4), 211-235.

McKee KL. (2011). Biophysical controls on accretion and elevation change in Caribbean mangrove ecosystems. *Estuar. Coast. Shelf Sci.* 91:475–83.

McKee, K. L., & Faulkner, P. L. (2000). Restoration of biogeochemical function in mangrove forests. *Restoration Ecology*, *8*(3), 247-259.

McKee, K. L., Feller, I. C., Popp, M., & Wanek, W. (2002). Mangrove isotopic (δ15N and δ13C) fractionation across a nitrogen vs. phosphorus limitation gradient. *Ecology*, *83*(4), 1065-1075.

McKee, K. L., Cahoon, D. R., & Feller, I. C. (2007). Caribbean mangroves adjust to rising sea level through biotic controls on change in soil elevation. *Global Ecology and Biogeography*, *16*(5), 545-556.

McKee, K., Rogers, K., & Saintilan, N. (2012). Response of salt marsh and mangrove wetlands to changes in atmospheric CO 2, climate, and sea level. In *Global change and the function and distribution of wetlands* (pp. 63-96). Springer, Dordrecht.

Mcleod, E., Chmura, g.l., bouillon, S., Salm, r., björk, M., duarte, C.M. *et al*. (2011). A blueprint for blue carbon: toward an improved understanding of the role of vegetated coastal habitats in sequestering CO_2. *Frontiers in Ecology and the Environment*, 9, 552–560.

Middleton, B. A., & McKee, K. L. (2001). Degradation of mangrove tissues and implications for peat formation in Belizean island forests. *Journal of Ecology*, *89*(5), 818-828.

Morris, J. T., Barber, D. C., Callaway, J. C., Chambers, R., Hagen, S. C., Hopkinson, C. S., ... & Wigand, C. (2016). Contributions of organic and inorganic matter to sediment volume and accretion in tidal wetlands at steady state. *Earth's future*, *4*(4), 110-121.

Muzuka, A. N., & Shunula, J. P. (2006). Stable isotope compositions of organic carbon and nitrogen of two mangrove stands along the Tanzanian coastal zone. *Estuarine, Coastal and Shelf Science*, *66*(3-4), 447-458.

NOAA National Ocean Service, 2017. Mean Sea Level Trend Key West, Florida. Available from. https://tidesandcurrents.noaa.gov/stationhome.html?id=8724580

Parkinson, R. W., DeLaune, R. D., & White, J. R. (1994). Holocene sea-level rise and the fate of mangrove forests within the wider Caribbean region. *Journal of Coastal Research*, 1077-1086.

Parkinson, R. W., Craft, C., DeLaune, R. D., Donoghue, J. F., Kearney, M., Meeder, J. F., ... & Turner, R. E. (2017). Marsh vulnerability to sea-level rise. *Nature Climate Change*, *7*(11), 756.

Phan, L. K., van Thiel de Vries, J. S., & Stive, M. J. (2014). Coastal mangrove squeeze in the Mekong Delta. *Journal of Coastal Research*, *31*(2), 233-243.

Pribyl, D. W. (2010). A critical review of the conventional SOC to SOM conversion factor. *Geoderma*, *156*(3), 75-83.

Radabaugh, K. R., Moyer, R. P., Chappel, A. R., Powell, C. E., Bociu, I., Clark, B. C., & Smoak, J. M. (2017). Coastal Blue Carbon Assessment of Mangroves, Salt Marshes, and Salt Barrens in Tampa Bay, Florida, USA. *Estuaries and Coasts*, 1-15.

Randazzo, A. F., & Jones, D. S. (Eds.). (1997). *The geology of Florida*. University Press of Florida.

Rivera-Monroy, V. H., & Twilley, R. R. (1996). The relative role of denitrification and immobilization in the fate of inorganic nitrogen in mangrove sediments (Terminos Lagoon, Mexico). *Limnology and Oceanography*, *41*(2), 284-296.

Rogers K, & Saintilan N. (2008). Relationships between surface elevation and groundwater in mangrove forests of Southeast Australia. Journal of Coastal Research 24: 63–69.

Saintilan N, Rogers K, Mazumder D, Woodroffe C. (2013). Allochthonous and autochthonous contributions to carbon accumulation and carbon store in

southeastern Australian wetlands. Estuarine, Coastal and Shelf Science 128: 84–92.

Sanders, C. J., Eyre, B. D., Santos, I. R., Machado, W., Luiz-Silva, W., Smoak, J. M., ... & Silva-Filho, E. (2014). Elevated rates of organic carbon, nitrogen, and phosphorus accumulation in a highly impacted mangrove wetland. *Geophysical Research Letters*, *41*(7), 2475-2480.

Sanders, C. J., Smoak, J. M., Naidu, A. S., Araripe, D. R., Sanders, L. M., & Patchineelam, S. R. (2010). Mangrove forest sedimentation and its reference to sea level rise, Cananeia, Brazil. *Environmental Earth Sciences*, *60*(6), 1291-1301.

Schmidt, M. W., Torn, M. S., Abiven, S., Dittmar, T., Guggenberger, G., Janssens, I. A., ... & Nannipieri, P. (2011). Persistence of soil organic matter as an ecosystem property. *Nature*, *478*(7367), 49.

Scholl, D. W., & Stuiver, M. (1967). Recent submergence of southern Florida: a comparison with adjacent coasts and other eustatic data. *Geological Society of America Bulletin*, *78*(4), 437-454.

Schumacher, B. A. (2002). Methods for the determination of total organic carbon (TOC) in soils and sediments.

Smith, T. J., Anderson, G. H., Balentine, K., Tiling, G., Ward, G. A., & Whelan, K. R. (2009). Cumulative impacts of hurricanes on Florida mangrove ecosystems: sediment deposition, storm surges and vegetation. *Wetlands*, *29*(1), 24.

Smoak, J. M., Breithaupt, J. L., Smith, T. J., & Sanders, C. J. (2013). Sediment accretion and organic carbon burial relative to sea-level rise and storm events in two mangrove forests in Everglades National Park. *Catena*, *104*, 58-66.

Stockmann, U., Adams, M. A., Crawford, J. W., Field, D. J., Henakaarchchi, N., Jenkins, M., ... & Wheeler, I. (2013). The knowns, known unknowns and unknowns of sequestration of soil organic carbon. *Agriculture, Ecosystems & Environment*, *164*, 80-99.

Stofberg, S. F., Essink, G. H. O., Pauw, P. S., De Louw, P. G., Leijnse, A., & van der Zee, S. E. (2017). Fresh Water Lens Persistence and Root Zone Salinization Hazard Under Temperate Climate. *Water Resources Management*, *31*(2), 689-702.

Stuiver, M., & Polach, H. A. (1977). Discussion reporting of 14 C data. *Radiocarbon*, *19*(3), 355-363.

Stuiver, M., Reimer, P.J., and Reimer, R.W., 2018, CALIB 7.1 [WWW program] at http://calib.org, accessed 2018-3-5

Törnqvist, T. E., González, J. L., Newsom, L. A., Van der Borg, K., De Jong, A. F., & Kurnik, C. W. (2004). Deciphering Holocene sea-level history on the US Gulf Coast: A high-resolution record from the Mississippi Delta. *Geological Society of America Bulletin*, *116*(7-8), 1026-1039.

Trumbore, S. (2009). Radiocarbon and soil carbon dynamics. *Annual Review of Earth and Planetary Sciences*, *37*, 47-66.

Twilley, R. R., Chen, R. H., & Hargis, T. (1992). Carbon sinks in mangroves and their implications to carbon budget of tropical coastal ecosystems. *Water, Air, and Soil Pollution*, *64*(1-2), 265-288.

Urrego, L. E., Correa-Metrio, A., González, C., Castaño, A. R., & Yokoyama, Y. (2013). Contrasting responses of two Caribbean mangroves to sea-level rise in the Guajira Peninsula (Colombian Caribbean). *Palaeogeography, Palaeoclimatology, Palaeoecology*, *370*, 92-102.

US climate Data. (2018). https://www.usclimatedata.com/climate/key-west/florida/united-states/usfl0244/2017/1.

Webb, E. L., D. A. Friess, K. W. Krauss, D. R. Cahoon, G. R. Guntenspergen, and J. Phelps. (2013). A global standard for monitoring coastal wetland vulnerability to accelerated sea-level rise. Nat. Clim. Chang. 3: 458–465. doi:10.1038/ nclimate1756.

Wdowinski, S., Bray, R., Kirtman, B. P., & Wu, Z. (2016). Increasing flooding hazard in coastal communities due to rising sea level: Case study of Miami Beach, Florida. *Ocean & Coastal Management*, *126*, 1-8.

Whelan KRT, Smith TJ III, Cahoon DR, Lynch JC, Anderson GH. (2005). Groundwater control of mangrove surface elevation: shrink and swell varies with soil depth. Estuaries 28: 833–843.

Woodroffe, C., Robertson, A., & Alongi, D. (1992). Mangrove sediments and geomorphology. *Tropical mangrove ecosystems. Coastal and estuarine studies*, *41*.

Woodroffe, C. D., Rogers, K., McKee, K. L., Lovelock, C. E., Mendelssohn, I. A., & Saintilan, N. (2016). Mangrove sedimentation and response to relative sea-level rise. *Annual review of marine science*, *8*, 243-266.

Woods Hole Oceanographic Institute. (2018). Radiocarbon dating methods and calculations. http://www.whoi.edu/nosams/radiocarbon-data-calculations.

Zimmerman, A. R., & Canuel, E. A. (2000). A geochemical record of eutrophication and anoxia in Chesapeake Bay sediments: anthropogenic influence on organic matter composition. *Marine Chemistry*, *69*(1-2), 117-137.

Appendix

Appendix 1: ^{14}C Age-Depth Model

The radiocarbon age-depth model constructed followed a monotonic pattern that exponentially regressed to the base of the core with limited age discrepancies (Fig. 29). With this model, we were able to: 1) establish an age range of when basal peat started forming at Snipe Key (6 ka BP; mid-Holocene), which is supported by plant macrofossils and $\delta^{13}C$ values (Table 5; Kahn et al., 2017), 2) calculate accumulation, accretion and OC burial rates, allowing for timescale comparisons. When the age-depth model was compared to the submergence curves of southern Florida (Scholl & Stuiver, 1967), similarities were seen between the radiocarbon dates and depths of the younger peats analyzed, however, beyond 3 m depth, the radiocarbon samples dated in this study were older than the ages found by Scholl & Stuiver, 1967 as associated depths. Further, the peat sequence of the study was 5 m in depth compared to the 4-m sequence that Scholl & Stuiver (1967) found before hitting bedrock, which could mean that mangroves have been established and burying carbon in the Lower Florida Keys longer than in the southern coastal Everglades.

The Snipe Key core radiocarbon profile yielded confounding results at the base of the core, which did not fit the general trend expected from the age-depth model (Fig. 16). When these base segments are removed the model fit improved to $R^2 = 0.92511$ (Fig. 29). Confounding results from basal peats can best be explained by two possible mechanisms that cause the base of the core to return an age that does not properly represent the true age of basal peat formation. First, under carbonate platforms, a freshwater lens often exists from rainwater steeping down pore space in the peat as well as possible discharge of

submarine groundwater, which will then float on top of the denser saltwater (Corbett et al., 2017; Stofberg et al., 2017). Due to the salinity gradient, the lens creates a different pore water chemistry than that found throughout the rest of the core. This can cause organic acids to form, breaking down both the basal peat section and the underlying carbonate basement, ultimately leading to small scale peat collapse at depth (Lazo et al., 2017). Second, the coring tool that is used to extract the soil samples from depths can create suction that can contaminate the bottom samples that already have low soil strength (Bird et al., 2004; Törnqvist et al., 2004). Due to these potential vectors of contamination, it is expected that the lowest three intervals dated from the Snipe Key peat sequence (485.5, 487.5 and 489.5 cm depth) should have ages that are older than what was actually measured via ^{14}C during this study. Hence, the deepest segment of the core (489.5 cm) most likely has an age closer to 6028 Cal yr BP, which calculated to a OC burial rate of 52.31 g m^{-2} yr^{-1} rather than the observed at 80.5 g m^{-2} yr^{-1} based on the confounding age measured. Based on the improved age-depth model after confounding results were removed, it is suspected that mangroves on Snipe Key became established and began burying peat an estimated 6 ka BP. To improve fit, confounding intervals were removed and a new exponential regression was applied (Fig. 29), giving an $R^2 = 0.92511$, $p < 0.0001$, yielding Eq. 16:

Equation 16. Adjusted regression equation for ^{14}C age-depth model

$$y = 43.920e^{0.0004x}$$

Appendix 2: Surface Elevation Tables

A lack of agreeance between radiometric dating (^{210}Pb) and time-series approach (SETs) was found in this study; this discontinuity has been observed in other studies (Parkinson et al., 2017; Breithaupt et al., 2018a). The mean SET change in surface elevation measured -0.67 ± 0.40 (Big Pine Key) and 1.06 ± 0.25 mm yr^{-1} (Sugarloaf Key) for the five-year time period represented (Fig. 30). It should be noted that the SETs in this study were not sampled each year since installation nor at the same time of year when sampled. Therefore, it is possible that these rates of change represent soil shrink/swell and/or erosion/deposition (Whelan et al., 2005; Rogers & Saintilan, 2008). The ^{210}Pb accretion rate was 5.57 ± 1.52 mm yr^{-1}, measured from the surface interval of the soil core retrieved from Big Pine Key (representing 2012 to 2015). This study's findings contradict Parkinson et al. (2017), who asserts that time-series approaches yield higher sedimentation rates than radiometric geochronologies, leading to overestimations of wetland resilience to SLR. The SET surface elevation change measurements are orders of magnitude less than the radiometric accretion rate found during this study. This finding that mean surface elevation change is lower than accretion rates compare well with findings compiled by Breithaupt et al. (2018a) for both southwest Florida and Louisiana rates of vertical change.

Accretion rates and surface elevation changes are recognized as representations of different processes, which measure different things, although they both measure a rate of change. This raises concerns of how comparable time-series approaches are to radiometric dating methods (Kaye & Barghoorn, 1964; Cahoon et al., 1995; Cahoon & Lynch, 1997; Breithaupt et al., 2018a). The time-series methodology used during this study did measure a change in rate, however, it is unclear to what extent, if any, deposition of sediment

contributed to this change. Without associated MHs to accompany SETs, the contributions of surface and subsurface processes to surface elevation change are not able to be identified (Webb et al., 2013). The lack of agreeance found between radiometric and SET rates, while the other geochronology measurements displayed the same rate at the associated depth, allows for this study to conclude, it is most representative to use the radiometric rates measured to interpret sedimentation and burial processes at these sites. However, data retrieved from SETs should not be disregarded, as this data can help understand variability in sub-annual and annual processes, which represent events like extreme tides and storms.